

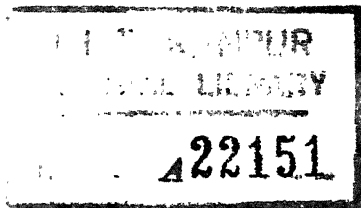
**DEFORMATION CHARACTERISTICS  
OF  
AUSTENITIC STAINLESS STEELS CONTAINING  $\gamma'$  PRECIPITATES**

**A THESIS  
Submitted in Partial Fulfilment of the Requirements  
For the Degree of  
MASTER OF TECHNOLOGY**

**By  
RAGURAM**

**to the**

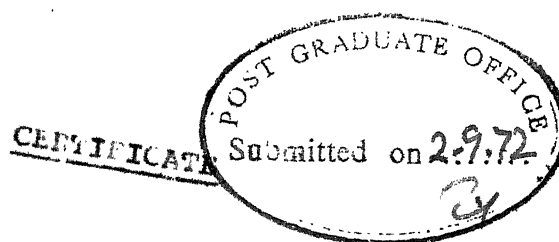
**DEPARTMENT OF METALLURGICAL ENGINEERING  
INDIAN INSTITUTE OF TECHNOLOGY, KANPUR  
SEPTEMBER, 1972**



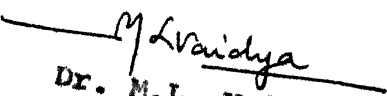
117442UR  
117442UR  
R 128

5 JAN 1973

ME-1972-M-RAG-DEF



This is to certify that the work described in this thesis, on "Deformation Characteristics of Austenitic Stainless Steels Containing  $\gamma'$  Precipitates", has been carried out under my supervision and has not been submitted elsewhere for a degree.

  
 Dr. M.L. Vaidya  
 Lecturer  
 Department of Metallurgical Engineering  
 Indian Institute of Technology, Kanpur

POST GRADUATE OFFICE  
 This thesis has been approved  
 for the award of the Degree of  
 Master of Technology (M.Tech.)  
 in accordance with the  
 regulations of the Indian  
 Institute of Technology Kanpur  
 Dated 13.8.72 24

ACKNOWLEDGEMENT

The author wishes to express his deep sense of gratitude to Dr. L.K. Singhal, for his able guidance and many fruitful discussions, that the author had from time to time.

He is thankful to Dr. M.L. Vaidya for many suggestions during this work.

He is extremely grateful to all those who have helped him in more than one way during this work.



## **ABSTRACT**

**A study of some of the mechanical properties of austenitic stainless steels containing particles has been made in this work. The properties examined are yield behaviour, work hardening, creep and a study of other deformation mechanisms. These have been done mainly through a detailed analysis of the dislocation motion. An attempt has been made to study critically various dislocation models existing. New mechanisms which overcome the defects of some of the earlier mechanisms have been outlined.**

# TABLE OF CONTENTS

Chapter	Title	Page
	CERTIFICATE	ii
	ACKNOWLEDGEMENT	iii
	TABLE OF CONTENTS	iv
	LIST OF TABLES	vi
	LIST OF FIGURES	vii
1	INTRODUCTION	1
2	MATERIALS AND METHODS	5
	2.1 Sample Preparation	5
	2.2 Experimental Methods	5
	2.2.1 Stress Relaxation Techniques	5
	2.2.2 Strain Rate Cycling Tests	8
	2.2.3 Work Hardening Rates	12
	2.2.4 Strain Rate Sensitivity	12
3	TENSILE YIELD	13
	3.1 Review	13
	3.2 Dislocation Sources and Bowing	15
	3.3 Modifications of Orowan's Approach	16
	3.4 Scope of the Present Work	20
	3.5 Yield Model	20
	3.6 Results	24
	3.7 Discussion	25
	3.8 Conclusion	32
4	WORK HARDENING AND INTERNAL STRESS	34
	4.1 Introduction	34
	4.2 Review	34
	4.3 Results	37
	4.3.1 Work Hardening Rates	37
	4.3.2 Internal and Effective Stresses	43
	4.4 Discussion	48

Chapter	Title	Page
5	MOTION OF PARTIAL DISLOCATIONS	55
5.1	Introduction	55
5.2	Theory	56
5.3	Results	58
5.4	Discussion	61
5.4.1	Effect of Stacking Fault Energy of the Precipitate ( $\gamma_p$ )	61
5.4.2	Effect of Orientation	64
5.4.3	Effect of Stacking Fault Energy of the Matrix ( $\gamma_m$ )	65
5.4.4	Effect of Antiphase Boundary Energy ( $\gamma_{apb}$ )	65
5.4.5	Effect of Drag Coefficient ( $D_p$ ) of the Precipitate	69
5.5	Present Model	69
6	CREEP DEFORMATION	74
6.1	Introduction	74
6.2	Review	74
6.2.1	Recovery Creep Theory	75
6.2.2	Slip Theories	76
6.3	Present Model	79
	REFERENCES	82
	APPENDIX-1	86
	APPENDIX-2	89
	APPENDIX-3	90
	APPENDIX-4	92
	APPENDIX-5	
	APPENDIX-6	

LIST OF TABLES

Table	Title	Page
1	Effect of aging treatment on precipitate size	6
2	Properties of v1682 alloy and NIMONIC PE16	19
3	Effect of antiphase boundary energy on Frank-Read stress and number of loops	31
4	Work hardening rates	44
5	Schmidt factors of the leading and trailing partials for different orientation	64

LIST OF FIGURES

Figure No.	Title	Page
1	Typical stress-strain and stress relaxation curves	9
2	Mechanisms proposed for the by pass of precipitates by dislocations. (a) Bowing in the slip plane, (b)-(d) cross slip at the precipitate	14
3	Variation of yield stress with the anti-phase boundary energy	26
4	Comparison of theoretical model with experimental results	27
5	Comparison of the present model with Ashby's theory	28
6	Strain rate sensitivity	29
7	Effect of volume fraction on yield stress	30
8	True stress - true strain curves for a) Specimen aged at 675°C for 20 hours b) Specimen aged at 675°C for 5 hours	38
9	True stress true strain curves for a) Samples aged at 675°C for 550 hours b) Samples aged at 675°C for 125 hours	39
10	True stress true strain curves for a) Samples aged at 725°C for 8 hours b) Samples aged at 725°C for 4 hours	40
11	True stress true strain curves for a) Samples aged at 725°C for 200 hours b) Samples aged at 725°C for 30 hours	41
12	True stress true strain curves for a) Samples aged at 750°C for 1000 hours b) Samples aged at 750°C for 200 hours	42

Figure No.	Title	Page
13	Plot of log true stress vs. log true strain for a) Samples aged at 675°C for 5 hours b) Samples aged at 675°C for 550 hours	45
14	Plot of log true stress vs. log true strain for a) Samples aged at 725°C for 4 hours b) Samples aged at 725°C for 8 hours	46
15	Work hardening rate as a function of aging time at a plastic strain of 4%	47
16	Effective and internal stresses obtained by stress relaxation as a function of the strain Sample aged at 675°C for 20 hours	49
17	Effective and internal stresses obtained by stress relaxation as a function of the strain Sample aged at 675°C for 20 hours	50
18	Effective and internal stresses obtained by stress relaxation as a function of the strain Sample aged at 725°C for 200 hours	51
19	Effective and internal stresses obtained by strain rate cycling as a function of the strain Sample aged at 725°C for 30 hours	52
20	Nature of the velocity of partial dislocations moving in a matrix containing precipitate	60
21	Effect of stacking fault energy of the precipitate on dislocation spacing (volume fraction = 0.1)	62
22	Effect of stacking fault energy of the precipitate on dislocation spacing for a volume fraction of 0.02	63
23	Effect of orientation on dislocation spacing	66
24	Effect of stacking fault energy of the matrix ( $\gamma_m$ ) on the dislocation spacing	67

Figure No.	Title	Page
25	Effect of antiphase boundary energy on dislocation spacing	68
26	Effect of drag coefficient of the precipitate $D_p$ on dislocation spacing	70
27	Bowing of partial dislocations	72

## CHAPTER 1

### INTRODUCTION

Austenitic stainless steels have been put to use in a number of places. It finds useful application as material for fuel element canning and in some components in power stations. The vast utility of this material is attributed mainly to its improved high temperature properties.

Standard austenitic stainless steels combine adequate corrosion resistance with ductility so that the steel can readily be formed. Although the strength can be considerably increased by cold working, ductility becomes too low to allow fabrication and the improved mechanical properties cannot be retained at elevated temperatures.

Refinements have been brought about to improve the properties of austenitic stainless steels. Addition of niobium has indicated a marked improvement in high temperature creep properties. A further improvement has been made by the addition of titanium (Irvine et. al. 1961) to produce precipitation hardened alloys in which particles of Ni-Ti phases are precipitated. The addition of titanium in certain quantities to austenitic stainless steels also helps to reduce embrittlement of the  $\gamma$  phase.



### The Iron - Nickel - Chromium - Titanium System

A detailed study of the system was done by Hattersley and Hume - Rothery (1965). The addition of titanium to stainless steels is usually made to fix carbon and so avoid susceptibility to intergranular corrosion resulting from chromium carbide precipitation at grain boundaries during certain heat treatments. Usually the titanium content in stabilised stainless steels is not less than five times the carbon percentage, but even so, it remains well within the solubility limit in that no additional phases of the Fe-Ni-Cr-Ti systems are formed by Ti in excess of that required to combine with carbon and nitrogen. When titanium is added deliberately to the extent that the solubility limit is exceeded, formation of  $\text{Ni}_3\text{Ti}$  precipitates on aging have been reported (Irvine et. al. 1961) in a steel containing 25% nickel, 15% chromium and around 3.5% titanium.

The hardening mechanism in these alloys is associated with the precipitation of an fcc precipitate based on the  $\gamma'$ - $\text{Ni}_3\text{Ti}$ . This precipitate is found to occur at peak hardness in all these alloys. (Mihalisin and Decker 1960). A feature of the  $\gamma'$  precipitate is that it is formed at very early aging times (Silcock and Williams 1966). The maximum response to aging for a given volume fraction of precipitate was a function of the misfit between the matrix and  $\gamma'$ .  $\gamma'$  is not necessarily the equilibrium precipitate, but

is generally formed at an intermediate stage in the aging process. The precipitation process in these steels is usually (Blackburn 1961)

Matrix  $\rightarrow$  zones  $\rightarrow \gamma' \rightarrow$  equilibrium precipitate

The morphology of  $\text{Ni}_3\text{Ti}$  was found to depend on the aging temperature; a cellular precipitate being produced at temperatures upto  $800^\circ\text{C}$  and a Widmanstatten precipitate above the temperature.

In austenitic stainless steels containing titanium, it has been shown that the overaging can be rapid due to the formation of a cellular precipitate of cph  $\text{Ni}_3\text{Ti}$  when titanium exceeds 3%. Steels containing less than 3% titanium show spherical precipitates of the  $\gamma'$  form of  $\text{Ni}_3\text{Ti}$  which only transforms to hexagonal  $\text{Ni}_3\text{Ti}$  very slowly in these steels. The growth of  $\gamma'$  precipitates is diffusion controlled (Clark and Pickering 1967) and the particle size increases with time at any given aging temperature according to a relation of the form

$$D = Q t^n + C \quad (1)$$

where  $D$  is the diameter of the precipitate in angstrom units,  $t$  is the time,  $Q$  and  $n$  are constants.

Scope of the present work.

In the present work the tensile yield behavior in a precipitation hardenable austenitic stainless steel containing  $\gamma'$  precipitates has been predicted on the basis of a model. The model has been extended to assess the creep rates. The order of the stresses in these materials and their work-hardening behaviour have been studied. The nature of dislocation movement has also been investigated.

## CHAPTER 2

### MATERIALS AND METHODS

#### 2.1 Sample Preparation:

Flat tensile samples of 0.5 cm x 0.06 cm cross-section and gauge length of 2.0 cm were prepared from an alloy of composition 24.4% Ni, 17.3% Cr, 1.96% Ti, 0.035% C, 0.018% N, 0.19% Si, 0.034% Mn, balance Fe. The samples were vacuum sealed in quartz tubes and solution treated at 1150°C for 3 hours followed by a rapid quench in water. Samples were then vacuum sealed in separate quartz tubes and were subjected to treatments to obtain different volume fractions and precipitate size (Table 1).

#### 2.2 Experimental Methods:

Tests were conducted to measure the yield stress, internal stress, effective stress and work hardening rate. One test was performed to find the strain rate sensitivity. The individual tests are detailed below.

##### 2.2.1 Stress Relaxation Techniques:

The stress relaxation experiments, due to Noble and Hull (1964), were performed to evaluate the effective and internal stresses in these materials. It was first suggested by Seeger (1957) that the shear stress for yield or flow of

TABLE 1

Effect of aging treatment on precipitate size and  
volume fraction

Aging Temperature (°C)	Volume Fraction	Aging Time (Hours)	Mean Precipitate Radius (Å)
675	0.035	5	12.9
		20	20.4
		125	37.4
		550	61.8
725	0.02	4	25
		8	35
		30	60
		200	110
750	0.018	10	75
	0.018	1000	230

a metal could be considered to consist of two components: one an athermal component  $\tau_u$ , which depends on temperature only through the shear modulus  $\mu$ , and the other the thermal component  $\tau^*$ , which depends on temperature  $T$  and strain rate  $\dot{\gamma}$

$$\tau = \tau^* (T, \dot{\gamma}) + \tau_u \quad (2)$$

The separation of  $\tau^*$  from the total flow stress  $\tau$  is usually accompanied by measuring  $\tau$  at various temperatures upto a sufficiently high temperature  $T_0$  above which all short range obstacles are transparent to dislocations (i.e.  $\tau^* = 0$ ). The total applied stress is then applied solely to overcoming the long range stress field.

The above method is reasonably accurate and has been successfully employed in several investigations. But it is doubtful whether this method can be extended indiscriminately for studying thermally activated deformation in metals and alloys containing metastable obstacles. The method would obviously fail if the metastable structure changes to a stabler structure below  $T_0$  where  $\tau_u$  is usually evaluated. To overcome this difficulty stress relaxation techniques have been used (Rodríguez 1968).

When a tensile test is interrupted, stress relaxation occurs since plastic deformation continues to take place as long as the applied stress is sufficiently high for the dislocations to move. Since the total strain

is constant, the plastic strain  $e_p$  that occurs during relaxation is matched by an elastic strain  $e_e$  i.e.

$$\frac{de_p}{dt} = - \frac{de_e}{dt} = - \frac{1}{E} \frac{d\sigma}{dt} \quad (3)$$

where  $E$  is the combined elastic modulus of the specimen and the machine and  $\sigma$  is the tensile stress. As the plastic strain rate is governed by the thermal component of stress,  $\sigma^*$ , stress relaxation occurs at a progressively decreasing rate and will practically be unobservable when  $\tau_u$  is approached, as shown in Fig. (1). Thus this technique was adopted to find the internal and effective stresses at different strains.

### 2.2.2 Strain rate cycling tests:

The strain rate cycling technique (Michalak 1965), is an alternate method employed to differentiate between the applied and the effective stress acting on the dislocations. This has been made possible by the application of the Johnston - Gilman (1959) velocity-stress relationship to the results. Based on experiments in which the average velocity of the dislocations have been measured by etch-pitting techniques (Johnston and Gilman 1959 and others) the velocity stress relationship is given by

$$\bar{v} \propto \tau^{*m^*} \quad (4)$$

where  $\bar{v}$  is the average velocity,  $\tau^*$  the effective shear stress and  $m^*$  is the dislocation velocity-stress exponent

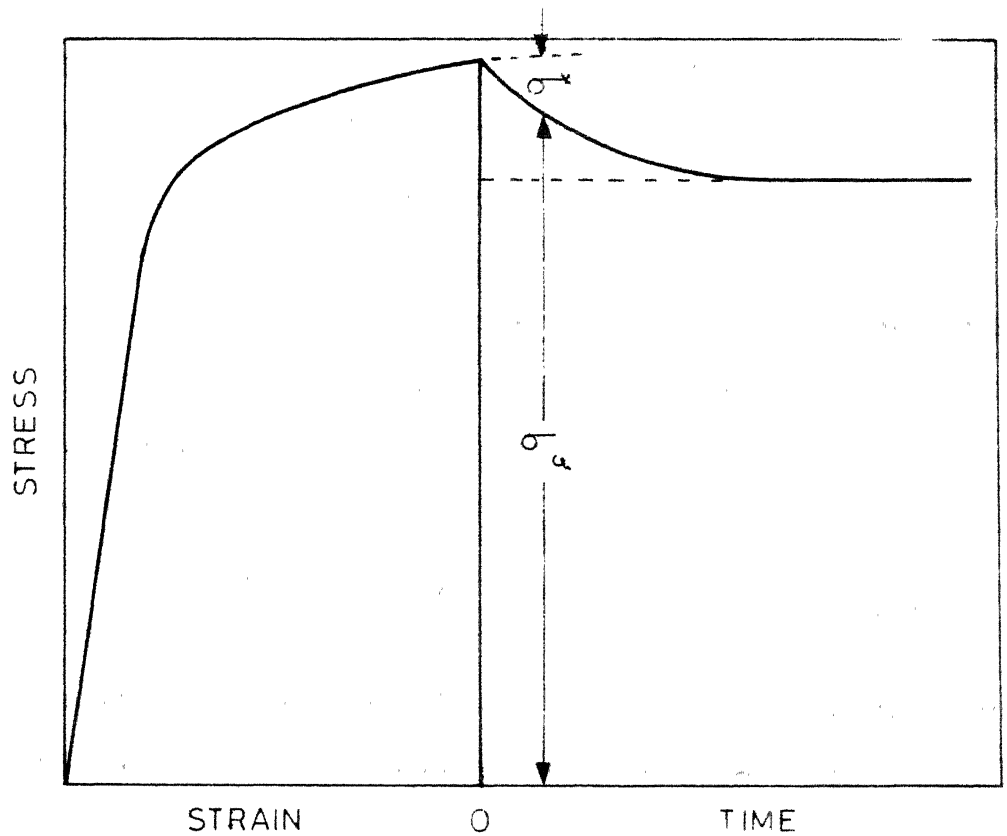


FIG.1 TYPICAL STRESS-STRAIN AND STRESS RELAXATION CURVES.



which is characteristic of the material and dependent on temperature. Since the shear strain rate is given by (Orowan 1940)

$$\dot{\gamma} = \rho b \bar{v} \quad (5)$$

where  $\rho$  is the density of mobile dislocations, and  $b$  the Burgers vector, it follows that

$$\dot{\gamma} = \rho b \tau^{* m^*} \quad (6)$$

If it is assumed that the density of mobile dislocations does not change during a given change in strain rate and there is no change in the dislocation structure during the change, then

$$\frac{\Delta \ln \dot{\gamma}}{\Delta \ln \tau^*} = m^* \quad (7)$$

at constant temperature and any strain. These assumptions are reasonable if the change in strain rate is not too great. It follows from eqn. (7) that

$$\ln \frac{\tau_2^*}{\tau_1^*} = \ln \frac{\tau_1^* + \Delta \tau}{\tau_1^*} = \frac{1}{m^*} \ln \frac{\dot{\gamma}_2}{\dot{\gamma}_1} \quad (8)$$

where  $\tau_2^*$  is the effective stress at strain rate  $\dot{\gamma}_2$  and  $\Delta \tau$  the change in applied stress resulting from a change in strain rate. Solving eqn. (8) for  $\tau_1^*$  gives

$$\tau_1^* = \Delta \tau / [(\dot{\gamma}_2 / \dot{\gamma}_1)^{1/m^*} - 1] \quad (9)$$

Since the effective stress is given by

$$\tau^* = \tau_A - \tau_i \quad (10)$$

where  $\tau_A$  is the applied stress and  $\tau_i$  is the internal stress, it follows that

$$\tau_i = \tau_A - \Delta\tau / [(\dot{\gamma}_2 / \dot{\gamma}_1)^{1/m^*} - 1] \quad (11)$$

The strain dependence of  $\tau_A$  and  $\Delta\tau$  may be obtained from normal tensile and strain rate cycling. Equations (10) and (11) are applicable on the assumptions that the Johnston-Gilman relation is valid throughout the deformation and that  $m^*$  is independent of strain.

The value of  $m^*$  required to evaluate  $\tau^*$  and  $\tau_i$  from strain rate cycling results according to eqn. (11), is best obtained from direct measurements of dislocation velocity by etch pitting. Alternately  $m^*$  could also be obtained from strain rate cycling (Johnston and Stein 1963). It was shown by them that

$$m = \frac{\Delta \ln \dot{\gamma}}{\Delta \ln \tau} \quad (12)$$

where  $\dot{\gamma}$  is the shear strain rate and  $\tau$  the applied stress.  $m$  increases with strain and  $m^*$  can be obtained by extrapolating to zero strain on a plot of  $m$  vs strain such that

$$m^* = [\Delta \ln \dot{\gamma} / \Delta \ln \tau^*] = [\Delta \ln \dot{\gamma} / \Delta \ln \tau]_{\dot{\gamma}=0} = m_{\dot{\gamma}=0} \quad (13)$$

### 2.2.3 Work hardening rates:

These were obtained from either the stress relaxation or strain rate cycling tests and no separate test was conducted for work hardening rates or work hardening index.

### 2.2.4 Strain Rate Sensitivity:

Strain rate sensitivity technique was originally proposed by Guard (1961) to evaluate the stress dependence of the dislocation velocity. This method consists of rapidly changing the strain rate during a normal tensile test and observing the changes in stress that result. The rate sensitivity exponent  $r$  may be derived from eqn. (5). Taking logarithms of both sides and differentiating with respect to stress ( $\sigma$ )

$$\frac{\partial \log \dot{\epsilon}}{\partial \log \tau} = \frac{\partial \log \rho}{\partial \log \tau} + \frac{\partial \log \bar{v}}{\partial \log \sigma} \quad (14)$$

The left hand side of the equation is equal to  $1/r$ , while  $\partial \log \bar{v} / \partial \log \sigma$  is a negligible quantity.

The strain rate sensitivity is obtained by plotting  $\Delta \sigma$  vs  $\Delta \dot{\epsilon}$  from a tensile test wherein a frequent change in the strain rate is effected.

## CHAPTER 3

### TENSILE YIELD

#### 3.1 Review:

The first attempt to explain the increased strength of materials with a second phase was made by Orowan (1948). Accordingly, a mechanism whereby dislocations could by-pass precipitates without shearing them was proposed, resulting in a dislocation loop being left in the glide plane around the precipitate (Fig. 2a). The increase in yield stress due to precipitates or strong dispersions has been termed as the Orowan stress. Classical Orowan loops in fact, have been observed in several iron base alloys (Bilsby 1966, Singhal and Martin 1968), nickel base alloys and copper base dispersion hardened alloys (Hirsch and Humphreys 1970).

An alternate method of dislocation by-pass was proposed by Hirsch (1957). The dislocation is considered to <sup>climb</sup>~~cross-slip~~ at the precipitate which, in the case of an edge dislocation (Fig. 2b) leaves a prismatic loop, whilst screw dislocations may or may not leave prismatic loops (Figs. 2c and 2d).

To obtain a quantitative estimate of the increase, it is essential to calculate the local stress  $\tau$  required to cause plastic flow on a microscopic scale. In essence, the problem is one of calculating the local stress to bend one dislocation between a pair of obstacles and thus to by-pass them.

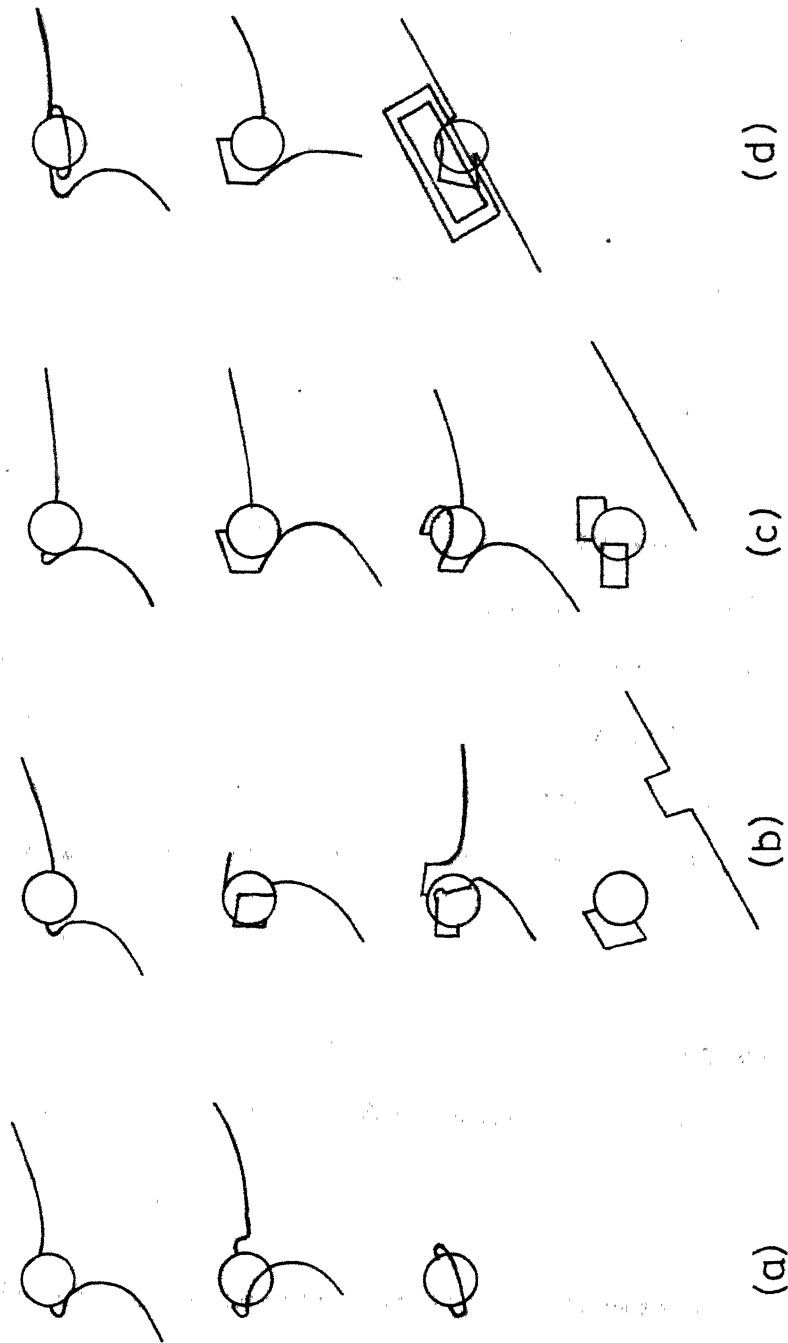


FIG.2 MECHANISMS PROPOSED FOR THE BY-PASS OF PRECIPITATES BY DISLOCATIONS. (a) BOWING IN THE SLIP PLANE. (b)-(d) CROSS SLIP AT THE PRECIPITATES.

### 3.2 Dislocation Sources and Bowing:

The dislocations move forward under the applied stress till their free motion is hindered by particles which obstruct their slip planes. But no source can operate until a stress is reached at which the dislocations bow between particles and thus by-pass them. According to Crowan (1948, 1954) the unit step in this micro-yielding is the bending of a segment of dislocation to a radius of curvature of half the interparticle spacing. The segment can then expand beyond the particles, thus by-passing them and leaving a dislocation loop around each one.

The total stress  $\tau$ , required to do this is roughly equal to the stress required to bend a dislocation to a semi-circle of radius  $D/2$ , where  $D$  is the space between particles in the slip plane through which the dislocation bulges.  $D$  may be obtained by calculating the interparticle separation  $2R_s$ . Assuming a random distribution of particles (Labusch)

$$2R_s = \frac{1}{2} \left( \frac{\pi}{f} \right)^{1/2} r_s \quad (15)$$

where  $f$  is the volume fraction of the precipitates and  $r_s$  is the mean particle radius. Thus stress  $\tau$  is

$$\tau \simeq \frac{2T}{bD} \quad (16)$$

where  $T$  is the line tension of the dislocation and  $b$  the Burgers vector.

Even if dislocations by-pass particles by the Orowan mechanism there exist other contributions to the microscopic yield stress besides these considered by Orowan. These could be due to atomic misfit, long range back stress due to misfit and positive difference in shear modulus, and also difference in elastic constants. These usually are small compared to the Orowan stress itself.

### 3.3 Modifications of Orowan's Approach:

In materials in which the yield stress is controlled by the Orowan mechanism, fair agreement has been obtained between experimental values of the yield stress and those calculated using formulae incorporating various modifications to the original Orowan equation. Significant among them has been that due to Hirsch and Humphreys (1970). They have assumed that the yield stress is controlled by obstacles weaker than the particles and as a first approximation have added the two contributions to the yield stress;  $\tau_m$  due to the matrix and  $\tau_p$  due to the particle, i.e.

$$\tau = \tau_p + \tau_m \quad (17)$$

This approach was also adopted by Ebeling and Ashby (1966) and Foreman and Makin (1967). The assumption of summing the two individual contributions is of uncertain validity. Actually a ~~maximum~~<sup>minimum</sup> stress is needed to bow a dislocation between two particles, which is analogous to the Frank-Read stress.

Ashby (1968) assumed that the bulging dislocation was a critical configuration, requiring the maximum applied stress when the two arms of the dislocation, on each side of the particle, first become parallel. On this basis it was suggested that a small forward displacement of the dislocation pulls out a dipole at each particle of width equal to the particle diameter  $x$ . The critical stress was assumed to be just that capable of elongating appropriate dipoles of width  $x$  spaced  $D$  apart. This led to two extreme values for the local stress required for by-passing,  $\tau_e$  for edge and  $\tau_s$  for screw where

$$\tau_e = \frac{1}{2\pi} \frac{Gb}{D} \ln \frac{x}{r_0} \quad (18)$$

$$\tau_s = \frac{1}{2\pi(1-\nu)} \frac{Gb}{D} \ln \frac{x}{r_0} \quad (19)$$

where  $r_0$  is the inner cut off radius,  $G$  the shear modulus and  $\nu$  the Poisson's ratio.

This model has a basic drawback in its assumption that the interaction between adjacement bowed out loops to be the critical configuration. A slightly better estimate may be obtained if  $D$  is replaced by  $\bar{D}$  in equations (18) and (19), where  $\bar{D}$  is the mean free distance between which the dislocation can bow out.

Li and Liu (1968) proposed a model for yield strength on the basis of circular dislocation pile-ups. To



begin with, in this model it is assumed that the innermost loop of radius  $r_1$  is stopped at the particle of a circular cross section. Loops are formed by the dislocations which can bulge through between particles by the Orowan mechanism. The applied stress is assumed sufficient to form the  $(n-1)^{th}$  loop and to form part of the  $n^{th}$  loop. Yielding is assumed to take place when the stress concentration  $(\tau_B)$  at the innermost loop is sufficient to yield or fracture the particle i.e. when the net stress  $\tau_1^*$  is equal to  $\tau_B$  where

$$\tau_B = \frac{\mu^* b}{30r_0} \quad (20)$$

$$\tau_1^* = \tau - \sum \tau_y + T \quad (21)$$

where  $\mu^*$  is the shear modulus of the particle,  $\tau$  the yield stress,  $\tau_y$  is the stress exerted by the  $j^{th}$  loop averaged over the  $i^{th}$  loop and  $T$  the line tension. The value of the yield stress  $\tau$  calculated thus is compared with the Frank-Read stress  $\tau_c$  where

$$\tau_c = \frac{\mu^* b}{2\pi L} \ln \frac{L}{r_0} \quad (22)$$

where  $L$  is the source length. The length  $L$  is the average separation between  $(n-1)$  loops before the formation of the  $n^{th}$  loop around each particle. The yield stress is taken as either  $\tau$  or  $\tau_c$  whichever is larger. The only drawback in this model is the arbitrary choice of  $\tau_B$  as in eqn. (20).

Though the agreement with experimental results is not too bad in the models described so far, they all predict a sharper decrease in yield stress as a function of particle size than the experimental observation (Singhal and Martin 1968, Silcock and Williams 1966).

Further more the expression for Orowan stress suggests that the yield stress is only a function of particle size and volume fraction. Nicholson (1971) suggested that particles are non-deformable, Orowan loops form around them and the intrinsic property of the particles were of no importance in determining the level of strength, provided that the particles are strong enough to force the dislocations to bow between them and eventually by-pass them. This does not appear to be the case. Despite smaller volume fraction the strength of the V1682 alloy in the overaged condition is higher than that of NIMONIC PE16 as can be seen from Table 2.

TABLE 2

Comparison of the strength of V1682 alloy and NIMONIC PE16

Alloy	Mean particle radius	Volume fraction	Anti phase boundary energy $\gamma_{APB}$	Increase in strength (MN/mm <sup>2</sup> )
V1682	80A°	0.07	300 erg/mm <sup>2</sup>	140
PE16	80A°	0.09	240 "	115

Due to a high Ti:Al ratio in V1682,  $\gamma_{APB}$ , the anti phase boundary energy of Ni<sub>3</sub>AlTi precipitate is higher and it appears

to influence the yield stress. It may be pointed out that Orowan loops were observed in both these alloys in the overaged condition (Raynor and Silcock 1970).

Finally the yield stress is experimentally found to be a function of strain rate. This indicates that a dynamic model is required to account for this effect whilst the static Orowan model fails on this count.

### 3.4 Scope of the present work

Taking into account the short comings experienced in the earlier models, an attempt has been made in this work to predict as accurately as possible the variation of yield stress with particle size. This has been done by accurately estimating the number of loops around each particle, the Frank-Read stress and stress concentration on the innermost loop. The effects of anti phase boundary energy and volume fraction have been studied. A comparison with some of the earlier models has also been made.

### 3.5 Yield Model:

The first step in the calculations is to determine whether the first loop can form at all. The critical stress  $\tau_{c1}$  to operate the Frank-Read stress is calculated using eqn. (22) with  $L = 2R_p - 2r_p$  where  $2R_p$  is given by eqn. (15) and  $r_p$  is the mean radius of the precipitate. An extra

factor  $1/(1-\nu)$  is to be used for screw dislocations. If the applied stress  $\tau$  is greater than  $\tau_0$  then the first loop can form. The radius of the first loop is taken to be equal to the precipitate radius.

The next step is to find the radii of the successive loops that encircle the first. In order to find this it is necessary to know the forces acting on the succeeding loops. The forces are

i) the applied shear stress  $\tau$  favouring the motion of the loop.

ii) the line tension which tends to drag the loop towards the centre. The line tension is given by (Li and Liu 1968)

$$L_t = \frac{A}{2r_i} \left\{ (1-\nu/2) \left( \ln \frac{8r_i}{r_0} - 1 \right) - \frac{1-2\nu}{8(1-\nu)} \right\} \quad (23)$$

where  $A = \mu b/2\pi(1-\nu)$ ,  $r_i$  is the radius of the loop in consideration, other terms having their usual significance.

iii) a stress ( $\tau_j$ ) repulsive in nature due to the inner loop.  $\tau_j$  is the shear stress produced by the  $j^{\text{th}}$  loop averaged over the loop of radius  $r_i$  outside the  $j^{\text{th}}$  loop and is given by (Li and Liu 1968),

$$\tau_j = \frac{A(2-\nu)}{r_i(r_i^2 - r_j^2)} \frac{r_j^2}{r_i} B\left(\frac{r_j}{r_i}\right) \quad (24)$$

where  $B$  is the complete elliptic integral of modulus  $r_j/r_i$  and  $r_j < r_i$  (Jahnke and Emde 1945).

The equilibrium condition can be described by the vanishing of the net stress  $\tau_i^*$  exerted on the  $i^{\text{th}}$  loop

$$\tau_i^* = \tau + \sum \tau_j + \frac{A}{2r_i} \left[ (1-\gamma/2) \left( \ln \frac{8r_i}{r_0} - 1 \right) - \frac{(1-2\gamma)}{8(1-\gamma)} \right] \quad (25)$$

where  $\tau$  is the applied stress. A summation has been indicated since the above eqn. (25) is very general in nature and can be used to find the radius of any loop. Equation (25) was programmed on an IBM 7044 computer and the radius so adjusted that  $\tau_i^*$  vanished within desirable accuracy. Calculations for the next loop is done in a similar way, but only after verifying whether the critical stress to form the second loop  $\tau_{c2}$  is less than  $\tau$ .

As a result of the formation of  $n$  loops, the stress on the innermost loop increases rapidly to such an extent that it begins to collapse. If it shrinks due to stress, it is simply gliding on the slip plane. However, in some cases it is possible that before the process of shrinkage occurs, the stress is high enough for the cross-slip to occur. When cross-slip occurs one or two loops will form near the precipitate depending on whether it is screw or edge dislocation. To find the velocity of the innermost loop, the forces acting on it just as it begins to shrink have to be considered. They are

- i) applied stress aiding the shrinkage.
- ii) line tension  $L_L$ , which changes continuously with the radius of the loop and accelerates the process of collapse.

iii) (n-1) loops surrounding the first, all tend to aid the motion of the innermost loop.

iv) As the innermost loop now enters the precipitate it has to create an antiphase region and this depends on the antiphase boundary energy  $\gamma_{APB}$  of the precipitate.

The velocity is now given by (Copley and Kear 1967)

$$v = v_s \exp \left( \frac{-D_p}{\tau_b + L_t b + (\sum \tau_j) b - \gamma_{APB}} \right) \quad (26)$$

where  $v_s$  is the shear wave velocity,  $D_p$  the drag coefficient of the precipitate. The line tension  $L_t$  is given by eqn. (23) and  $\tau_j$  is now

$$\tau_j = \frac{A(2 - \nu) r_j}{(r_j^2 - r_i^2)} E \left( \frac{r_i}{r_j} \right) \quad (27)$$

where  $E(r_i/r_j)$  is the complete elliptic integral of modulus  $(r_i/r_j)$  and  $r_i < r_j$  (Jahnke and Emde 1945).

Using the velocity, the strain rate  $\dot{\epsilon}$  is calculated

$$\dot{\epsilon} = \phi \rho b v \quad (28)$$

$\phi$  being a geometric quantity,  $\rho$  the mobile dislocation density and  $v$  the velocity of the innermost loop from eqn. (26). The strain rate thus obtained is compared with the applied strain rate.

The following criterion for yielding has been adopted; the value of Frank-Read stress which is required to

form the last of the minimum number of loops for achieving the desired strain rate gives the yield strength. It is assumed that the time taken by a loop to shrink is equal to the time taken for a dislocation to traverse from one particle to the next. It is important to note that while Li's model (Li and Liu 1968) allows the maximum number of loops to form, it is claimed in this model that only that many loops are sufficient wherein yielding is obtained at the lowest stress. It must be emphasized that having known precisely the number of loops that can form, the Frank-Read stress is calculated.

Calculations were carried out using the following constants:  $\mu = 6000 \text{ kg/mm}^2$ ,  $b = 2.54\text{\AA}$ ,  $r_0 = 2.54\text{\AA}$ ,  $\nu = 0.33$ ,  $v_s = 2.52 \times 10^5 \text{ cm/sec.}$ ,  $f = 0.018$ ,  $D_p = 867 \text{ dynes/cm}$ ,  $\gamma_{APB} = 280 \text{ ergs/cm}^2$ . At any one particle size different applied stresses tried to give corresponding loop radii and Frank-Read stress. In each case the velocity of the loop and hence the strain rate were calculated so as to be able to predict as accurately as possible the yield stress. The nature of the calculations for just one particle size have been shown in Appendix 1. The whole procedure was carried out for about thirty five particle sizes to obtain a plot of yield stress vs. particle size. The calculation of time for shrinkage of a loop is shown in Appendix 2.

### 3.6 Results:

Based on the above model a plot of average particle radius ( $r_v$ ) vs.  $2 \times \tau_c$ , where  $\tau_c$  is the critical stress, is

shown in Fig. (3). The results clearly show a gradual drop in the critical stress as the particle size increases. The drop in stress is fairly sharp upto about  $175\text{\AA}$ . While later the curve flattens considerably. By reducing the anti-phase boundary energy ( $\gamma_{\text{APB}}$ ), the whole curve was shifted to lower stress values. Calculations were carried out for four different  $\gamma_{\text{APB}}$ 's viz. 280, 240, 200, 160 ergs/cm<sup>2</sup>. A comparison of the values obtained by this model with these obtained experimentally has been shown in Fig. (4). A comparison has also been made between Ashby's theory and this work in Fig. (5). The results of the strain rate sensitivity test is shown in Fig. (6). The effect of volume fraction on the critical stress, Fig. (7), is to shift the curve up for increasing volume fraction.

### 3.7 Discussion:

The gradual decrease in the critical stress predicted by most theories is obtained. The steep fall in the initial stages Fig. (3), corresponds to the regions where only one loop exists. Once, more than one loop forms the drop is much more gradual. While the effect of  $\gamma_{\text{APB}}$  is shown to bring down the stress values another implication as a result of this is, the change in the number of loops for different  $\gamma_{\text{APB}}$ 's but at the same particle size. To illustrate this point values are shown in Table (3).



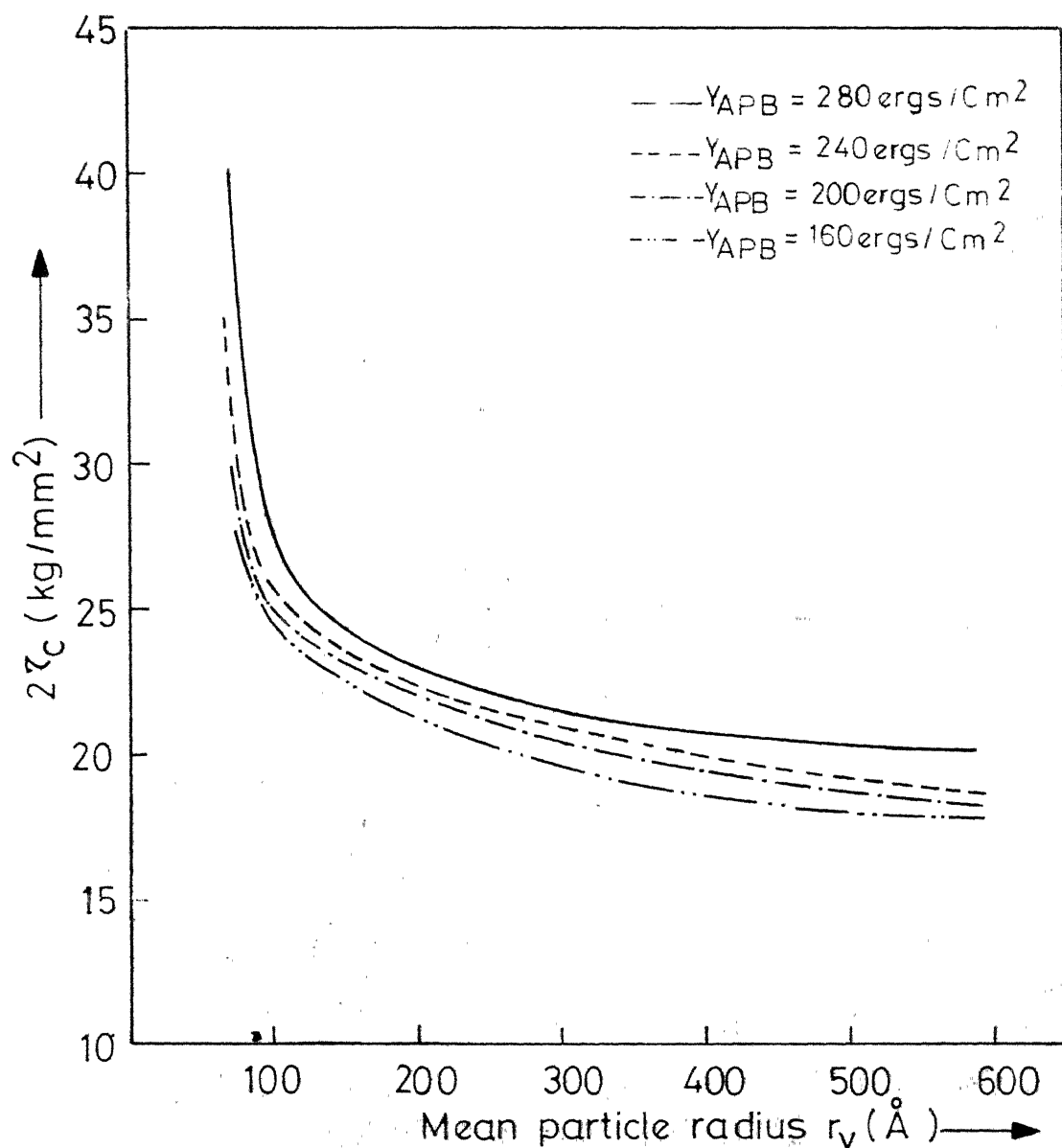


FIG. 3. VARIATION OF YIELD STRESS WITH ANTI-PHASE BOUNDARY ENERGY. (Volume fraction=0.018)

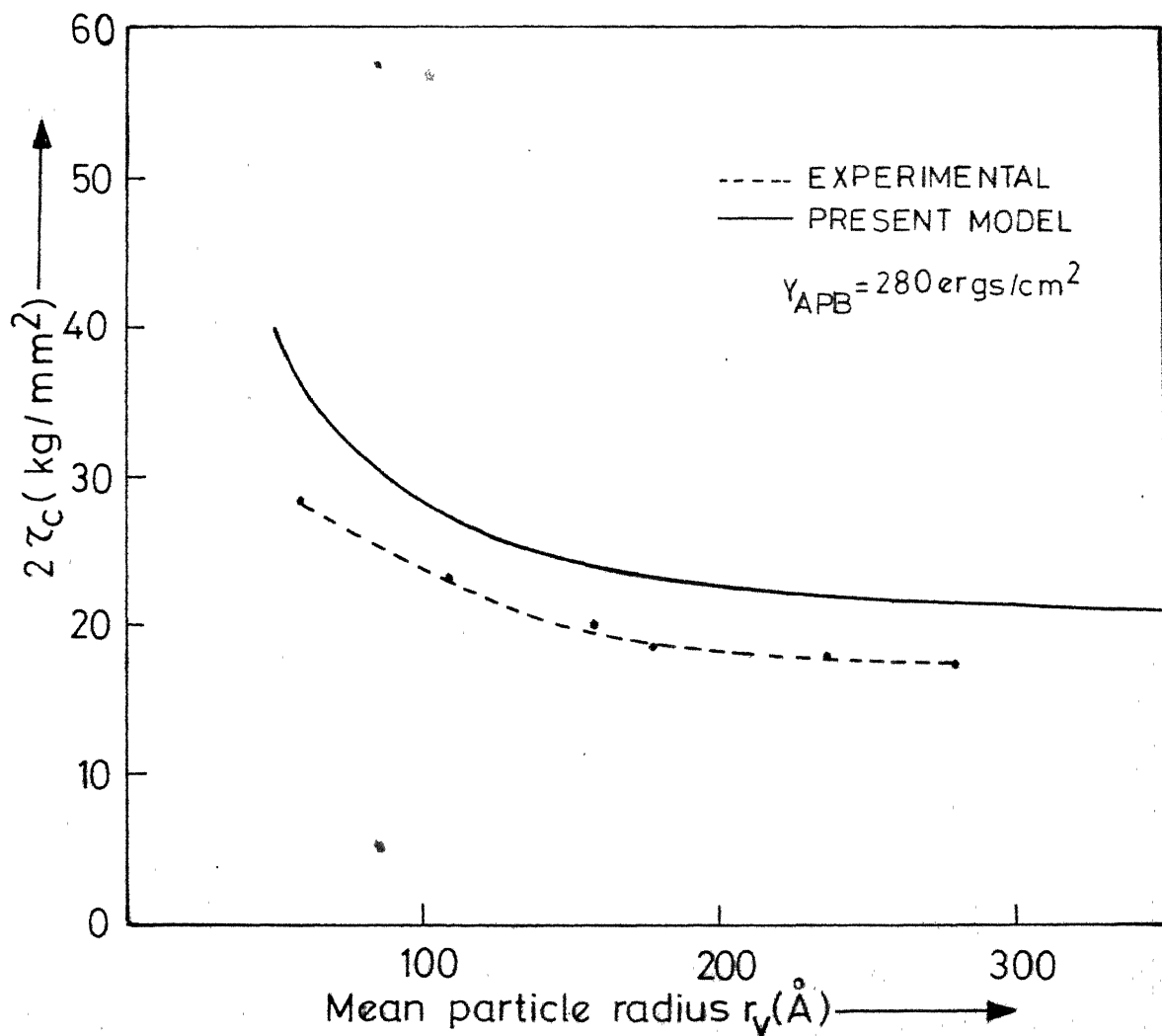


FIG.4. COMPARISON OF THEORETICAL MODEL WITH EXPERIMENTAL RESULTS.

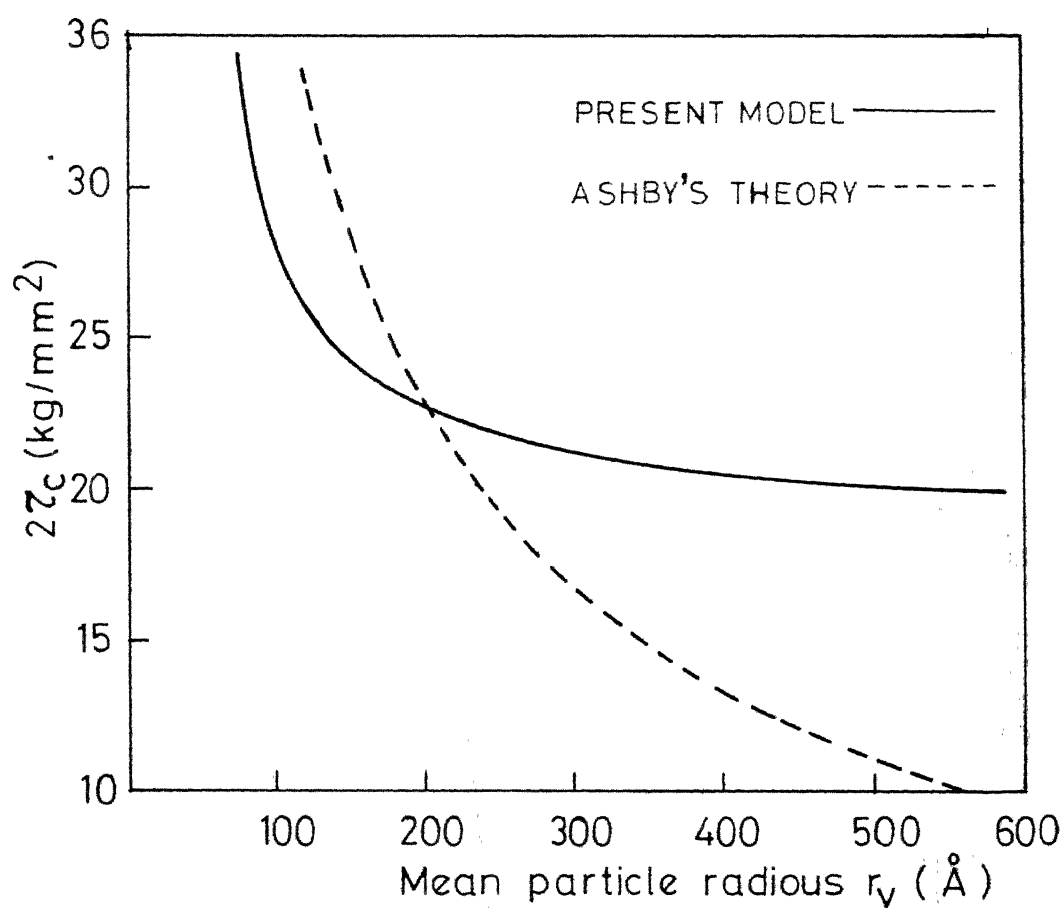


FIG. 5 COMPARISON OF PRESENT MODEL WITH ASHBY'S THEORY.

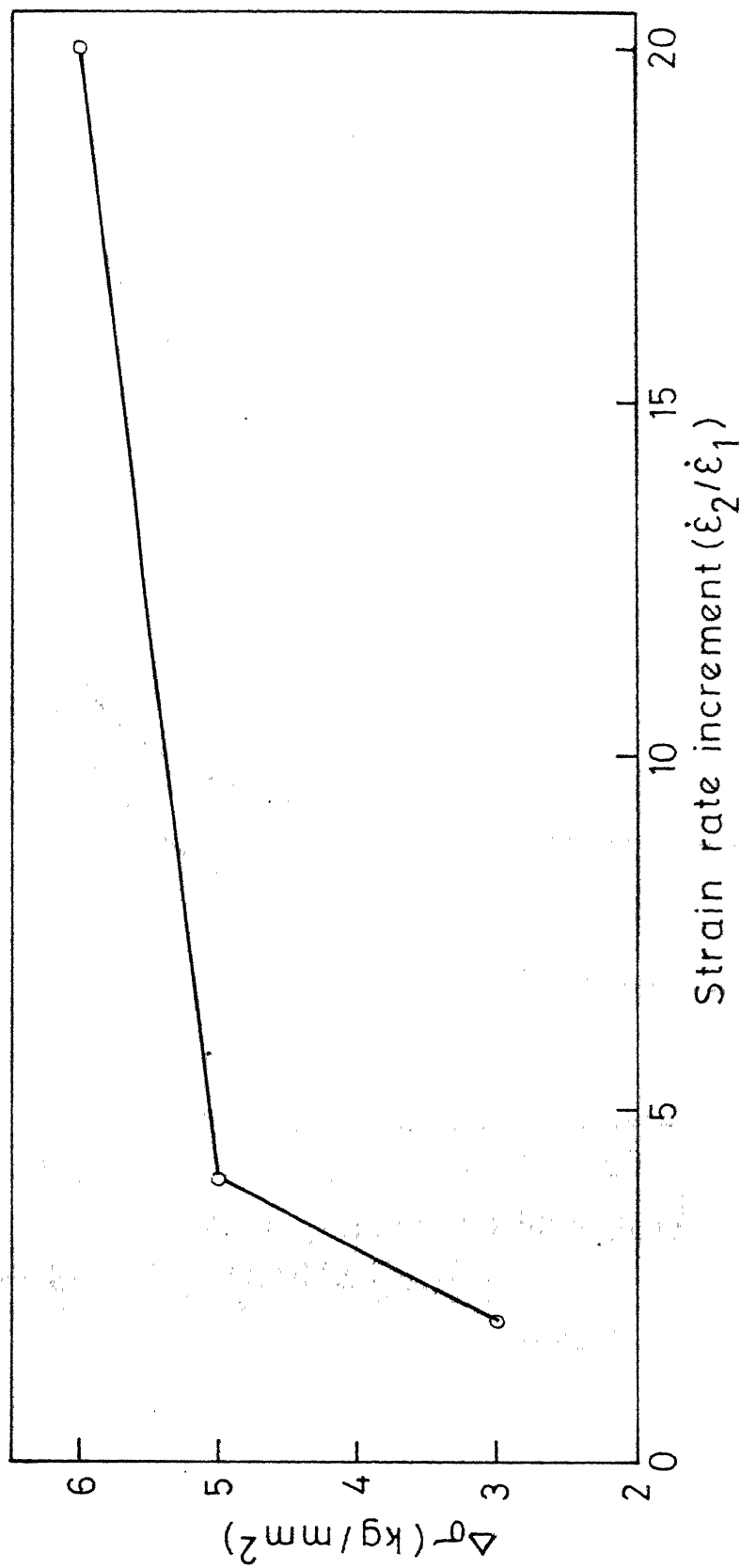


FIG.6. STRAIN RATE SENSITIVITY.

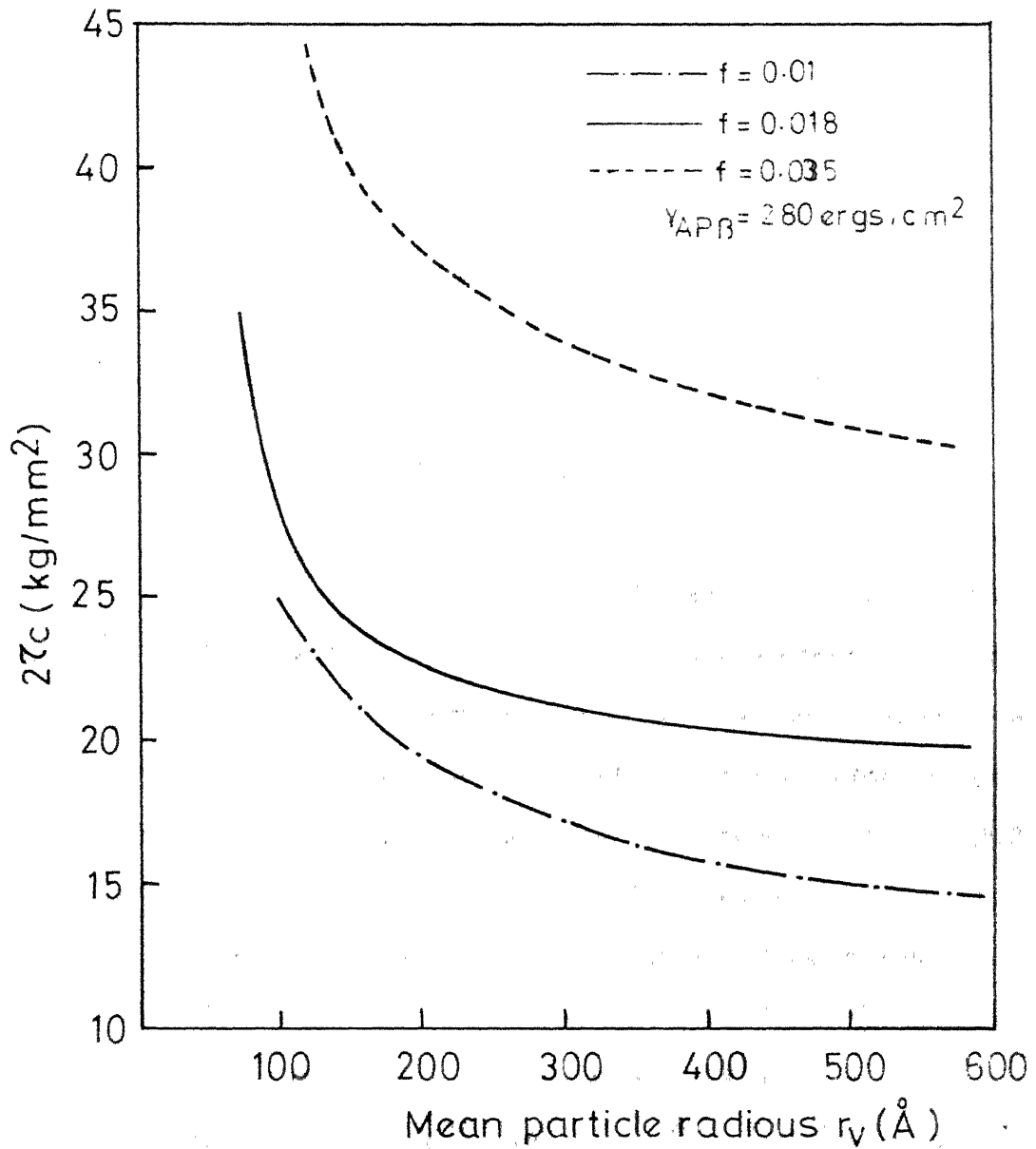


FIG.7. EFFECT OF VOLUME FRACTION( $f$ ) ON YIELD STRESS

TABLE 3

Effect of antiphase boundary energy on Frank-Read stress and number of loops.

Particle size		$\gamma_{APB}$ (ergs/cm <sup>2</sup> )	Number of loops	$2\tau_c$ (kg/mm <sup>2</sup> )
$r_s$	$r_v$			
480	588	280	4	20
		160	2	15.84

$$\text{where } r_v = (3/2)^{1/2} r_s \quad (29)$$

due to Gleiter and Hornbogen (1965).

Comparison with experimental values Fig. (4), shows a very close agreement with those predicted by this model. Below 100A° the gradient is much greater resulting in a sharp deviation from experimental values. This can be attributed to the fact that in this particle size range the effect of straight dislocation becomes important and expressions to include the interaction of straight dislocations with the shear loop must be considered. When there are at least two loops the effect of a straight dislocation would drastically be reduced. This shows that the model would predict values accurately when more than one loop is present. Figure (4) shows values of  $r_v$  upto 300A° only since experimental values beyond 300A° were not available. But the trend clearly shows that the agreement would be good even beyond 300A°.

A comparison with Ashby's model indicates a great difference in the slopes obtained by the two models. While

the values from Ashby's model seem to diverge away from the experimental points, the prediction of this model is more realistic.

The results of the strain rate sensitivity tests (Fig. 6) clearly show the expected variation in a plot of instantaneous change of stress  $\Delta\sigma$ , vs. the strain rate. It may be mentioned that such a behaviour has also been reported in a ferritic Fe, 2.5% Si, 1.4% Ti alloy containing ordered  $\text{Fe}_2\text{SiTi}$  precipitates (Papaleo and Whiteman 1971).

The effect of increasing the volume fraction of the precipitate is to increase the yield stress (Fig. 7). This could be expected considering the fact that an increase in the volume fraction results in a decrease in the inter-particle spacing for the same particle size. Thus it would be increasingly difficult to bow the dislocation between two particles of a much lower spacing, the major resistance to bowing being the line tension, since the line tension is inversely related to the radius of curvature while bowing.

### 3.8 Conclusion:

While this model can be claimed to be a vast improvement over the earlier models on the basis of its accurate prediction of  $\tau_c$  and the good agreement with experimental results, it has some drawbacks. The effect of a straight dislocation on the shear loop has not been considered

in this model. This becomes important at small particle sizes. Such a consideration would effect a better correlation with the experimental values. Finally, this model, though applied only to the case of austenitic stainless steels containing  $\gamma'$  phase, in view of its generality, can be applied to any system having a coherent ordered precipitate where looping occurs.



## CHAPTER 4

### WORK HARDENING AND INTERNAL STRESS

#### 4.1 Introduction

While the tensile yield behaviour represents only one aspect of deformation, a better understanding is possible by examining the work-hardening behaviour also. This differs from the conventional theories of work hardening in single phase materials in that austenitic stainless steels containing the hard  $\gamma'$  phase, deformation occurs when the matrix shears plastically. An attempt has been made to examine the true stress-strain curves, the work hardening rates and internal stress in these materials.

#### 4.2 Review

The hardening effect produced by precipitate particles which depends both on precipitate size and spacing was first noticed by Merica et al (1921) during studies of the age hardening of duralumin. Jeffries and Archer (1921) suggested that the precipitate particle acted to block crystallographic slip. Mott and Nabarro (1940) estimated the yield strength in terms of the strains produced by precipitation and the increased stress required to force dislocations through adversely strained material. A theory of the dependence on spacing was proposed by Orowan (1948), who showed that the stress required to force a dislocation between two precipitates

The first attempt to quantitatively describe the hardening of metals by dispersions was by Fisher, Hart and Pry (1953). The theory assumed that dislocations were blocked by the dispersed particles and had to bow between them according to Orowan's description, resulting in the initial Orowan yield stress and in the process necessarily leaving behind dislocation loops about the particles. The loops would exert a back stress on the slip plane raising the level of applied stress needed to continue further slip. The accumulation of loops would continue until a limiting stress in or about the particle was reached after which the number of trapped loops would remain at that saturation level. The resultant saturation back stress was identified as the maximum hardening increment. This theory had some defects in the assumption that the back stress was thought to affect Frank-Read sources in the slip plane. These were considered to determine the matrix flow stress, while the Orowan stress seemed to be an independent stress determining mechanism. It was not clear whether the Orowan stress should be considered alternative to the matrix flow stress or in some way additive to it. Hence this theory was limited to estimating the maximum hardening effect at strains large enough that the Orowan stress was negligible.

Ashby (1966) suggested that the long range stresses broke down by plastic relaxation, in the matrix, of the large

stresses in and around each particle. A plastic shell forms round each particle and spreads outwards as straining proceeds, filling the volume between particles with secondary dislocations, which in general intersect the primary slip system. A glide dislocation must now cut through these secondary dislocations and also overcome long range back stresses from the particles in order to move. This approach was known as the secondary slip theory. This theory has a drawback in that an average dislocation density which assumes a uniform distribution has been assumed, which is in general incorrect.

Hirsch and Humphreys (1970) with the aid of electron microscopy developed a theory of work hardening on the following model: The glide dislocations interact with the particles and by a mechanism of cross slip generate as prismatic loops per dislocation. The loops are arranged in rows at the particles, form helices with screw dislocations and act as parallel linear obstacles whose lengths increase with increasing strain. This mechanism leads to a self-hardening of a slip line i.e. for a given slip line the flow stress increases with the number of dislocations emitted by the source. The self-hardening law has been computed. In addition the dislocations must be able to by pass other dislocations on adjacent glide planes (interaction hardening); the total flow stress being the sum of the self and interaction terms. The theory predicts a work hardening curve which is parabolic above an initial region of low hardening and explains the observed dependence on volume fraction and particle radius.

A more recent theory has been due to Hart (1972). This is an improvement of an earlier theory by Fisher et al (1953). This theory assumes that the Orowan stress is simply additive to the matrix flow stress and that the effect of the back stress from trapped loops is to raise the critical stress for bowing additional loops between particles. It also supposes that the normal strain hardening of the metal matrix proceeds in substantially the same way as it would without the dispersions. In addition to a quantitative evaluation of the dispersion hardening increment, it also predicts an initially constant value for the hardening increment over a strain interval that depends on particle size.

### 4.3. Results

#### 4.3.1 Work hardening rates:

Tests on tensile samples were conducted using an Instron machine using a constant cross-head speed of 0.02 cm/min. The true stress-strain curves for all the samples are shown in Figs. (8-12). The yield stress of the solution treated alloy being  $13 \text{ kg/mm}^2$ , the marked strengthening as a result of aging is clearly seen in all aged samples. Maximum strengthening was observed after 125 hours at  $675^\circ\text{C}$  but aging at  $750^\circ\text{C}$  for 200 and 1000 hours promoted overaging.

The work hardening rate, which is the slope of the true stress strain curve in the plastic region has been calculated for all samples at plastic strains of 1%, 4% and 12%. The

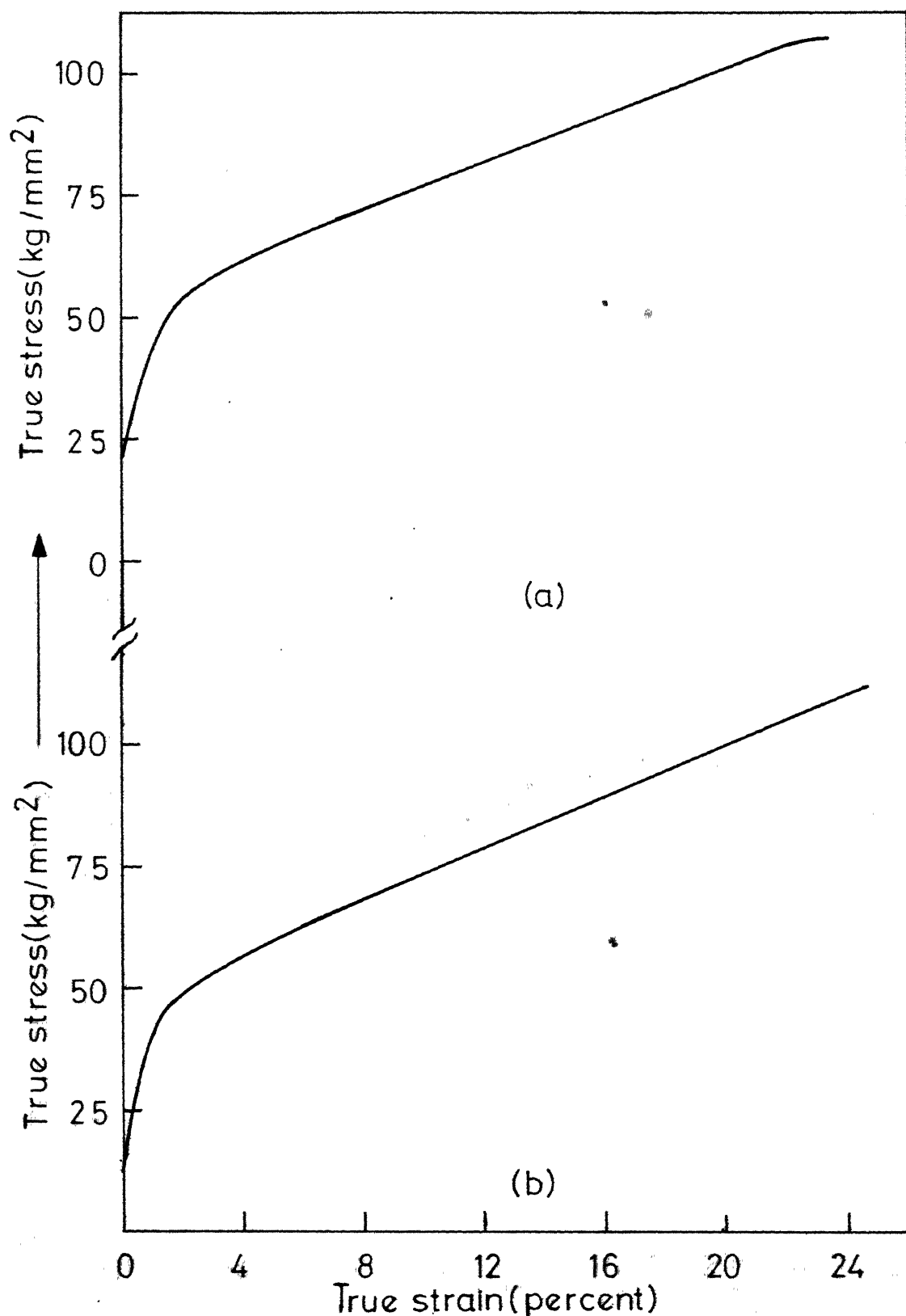


FIG 8. TRUE STRESS-TRUE STRAIN CURVES FOR  
(a) SAMPLE AGED AT 675°C FOR 20 HOURS.  
(b) SAMPLE AGED AT 675°C FOR 5 HOURS.

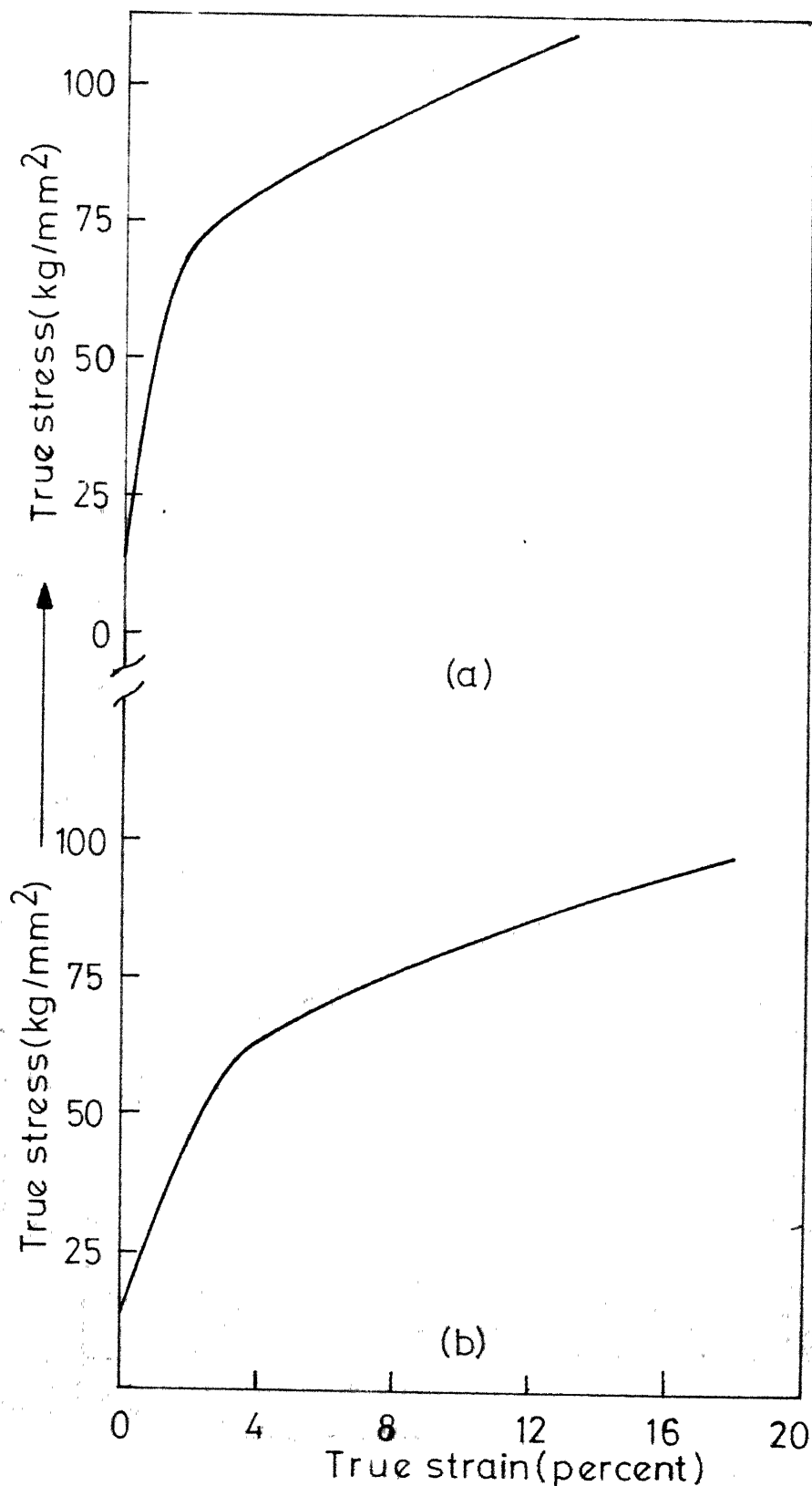


FIG 9 · TRUE STRESS-TRUE STRAIN CURVES  
FOR (a) SAMPLE AGED AT 675°C FOR 550 HOURS  
(b) SAMPLE AGED AT 675°C FOR 125 HOURS.

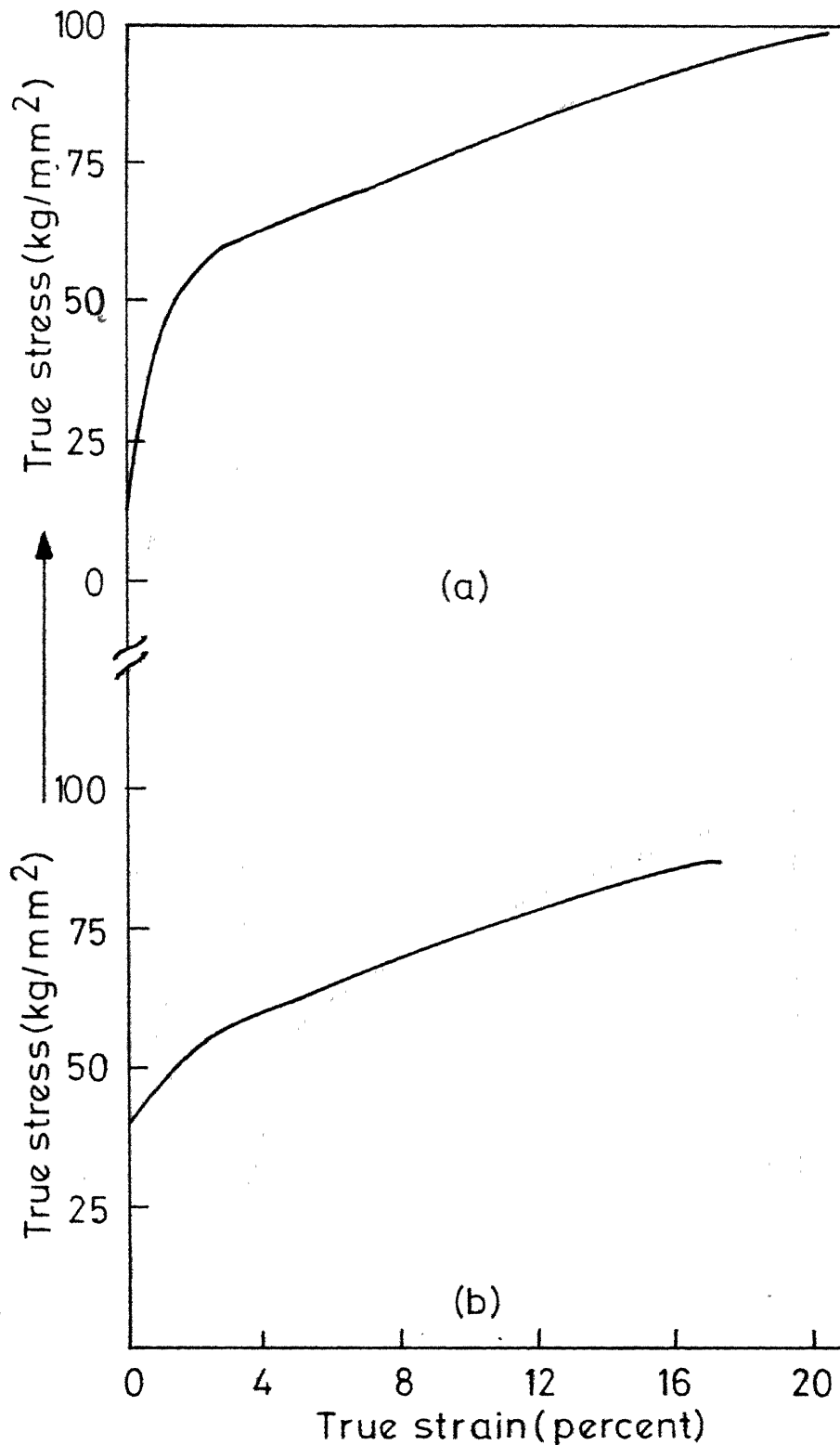


FIG.10. TRUE STRESS-TRUE STRAIN CURVES FOR  
(a) SAMPLE AGED AT 725°C FOR 8 HOURS.  
(b) SAMPLE AGED AT 725°C FOR 4 HOURS.

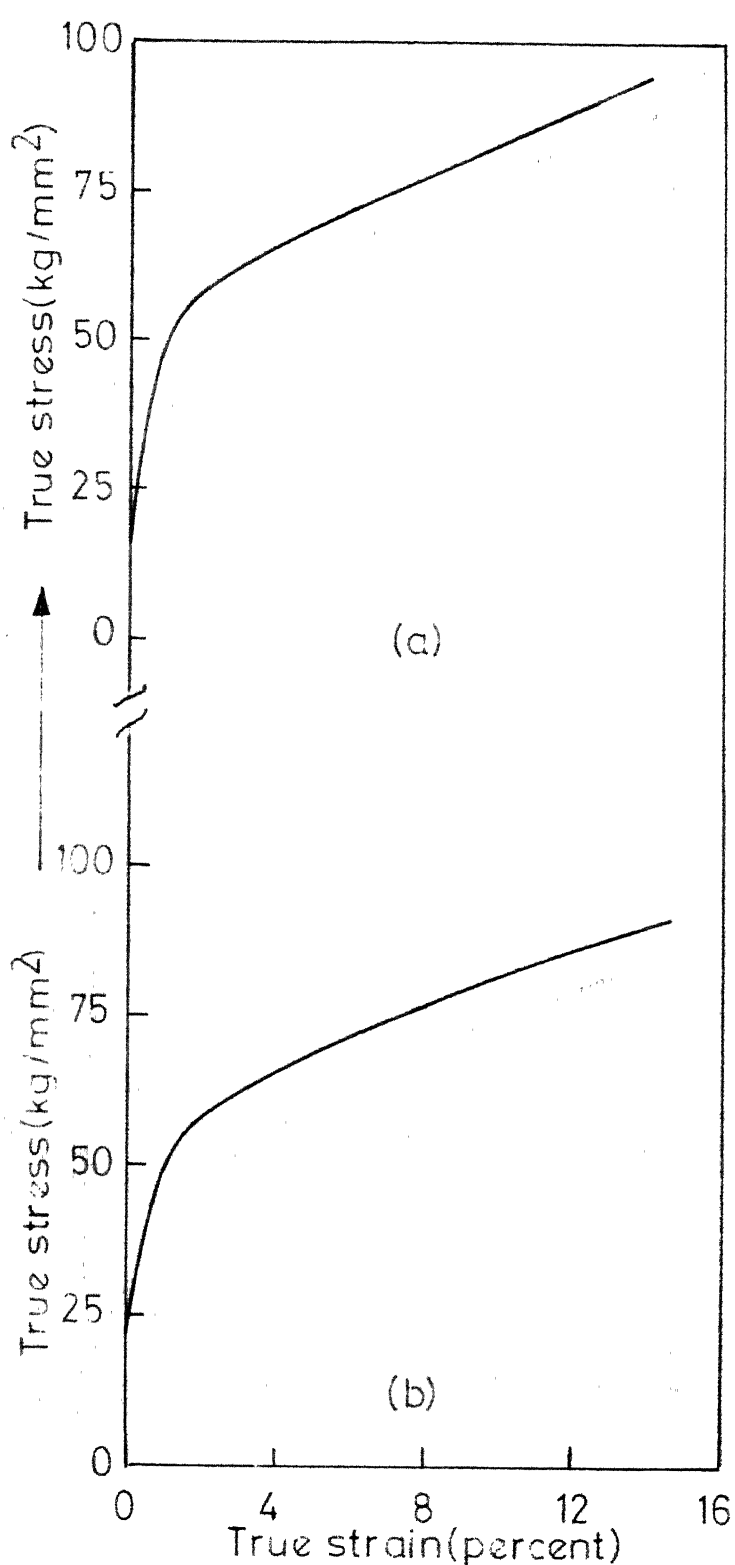


FIG.11. TRUE STRESS TRUE STRAIN CURVES FOR  
 (a) SAMPLE AGED AT 725°C FOR 200 HOURS.  
 (b) SAMPLE AGED AT 725°C FOR 30 HOURS



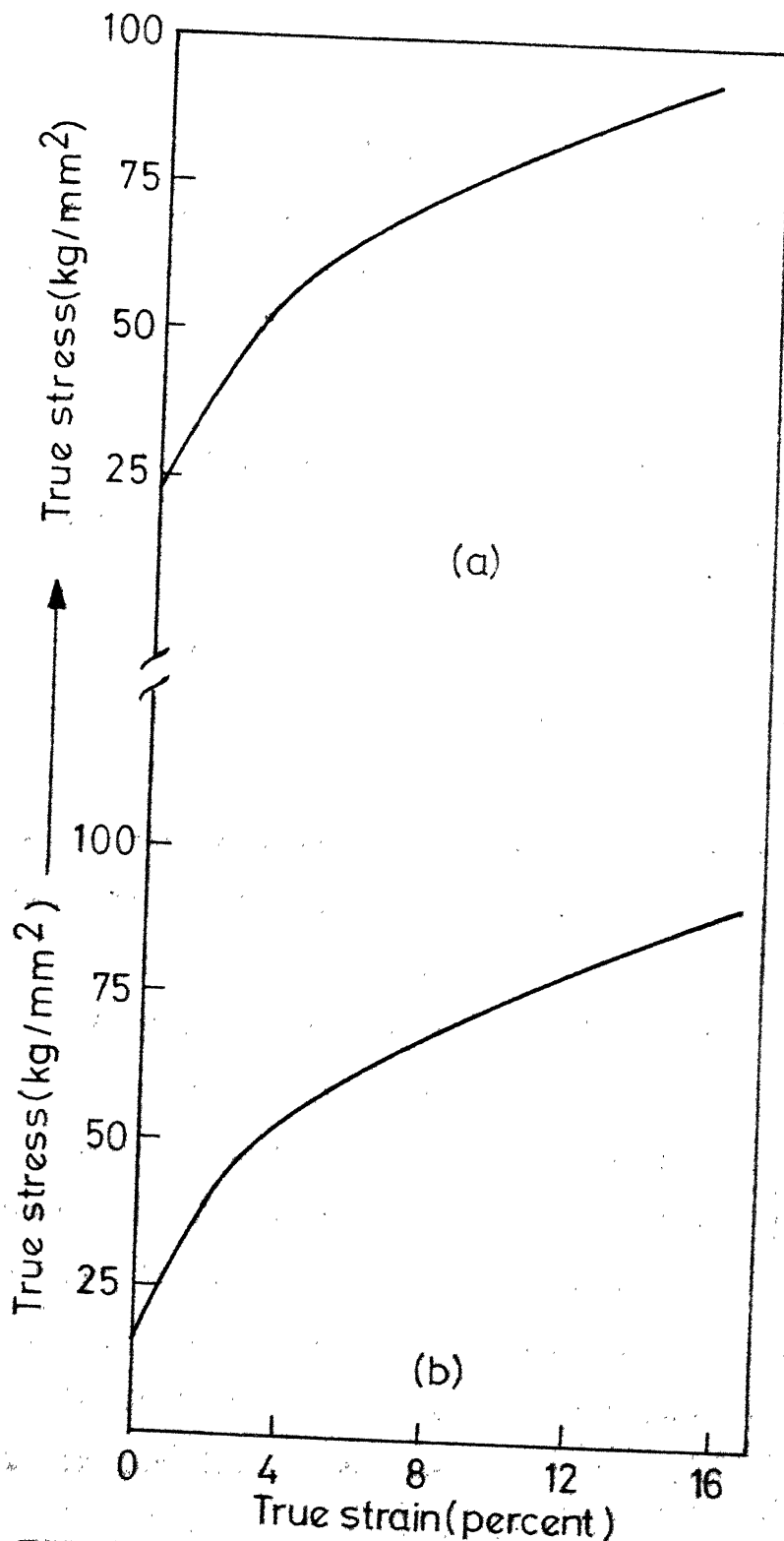


FIG.12 TRUE STRESS TRUE STRAIN CURVES FOR  
(a) SAMPLE AGED AT 750°C FOR 1000 HOURS.  
(b) SAMPLE AGED AT 750°C FOR 200 HOURS.

work hardening rate at 4% plastic strain has been plotted as a function of aging time for two volume fractions (Fig. 15). The work hardening rates are shown in Table (4). While the work hardening rates at the higher strain were all of the same magnitude, the initial rates were quite different. In the overaged condition rapid initial work hardening rates were observed. The table also shows the work hardening index which was obtained as the slope of the log true stress - log true strain plot. Work hardening index for four samples are shown in Figs. (13) and (14).

Deformation in the underaged alloys is usually by the movement of paired super-dislocations (Bilsby 1966, Singhal and Martin 1968). With increasing deformation, pile-up or planar arrays form (Wilson and Pickering 1969) indicating that cross slip was restricted.

In cases where the dislocation loops around  $\gamma'$  particles form, which represents the overaged condition, well defined stacking faults have been observed (Wilson and Pickering 1969). This indicates a significant lowering of the stacking fault energy of the precipitate. The precipitation of  $\gamma'$  removes large amounts of nickel from the austenitic matrix. In spite of overaging,  $\gamma'$  particles are largely coherent in the undeformed condition (Philips 1967).

#### 4.3.2 Internal and Effective stress:

The internal and effective stresses detailed in section (2.2), were obtained from stress relaxation and strain

TABLE 4

## Work Hardening Rates

Volume fraction	Aging Temp. (°C)	Aging Time (Hrs.)	Work hardening rates (Kg/mm <sup>2</sup> ) at plastic strains of			n
			1%	4%	12%	
.035	675	5	1250	312.5	250	0.5
		20	1562	312.5	250	0.4
		125	1458	469	188	0.28
		550	3125	417	250	0.32
.02	725	4	625	250	179	0.35
		8	1375	277	209	0.33
		30	1318	312	227	0.3
		200	1625	397	278	0.3
.018	750	200	1188	438	275	0.43
		1000	2160	513	270	0.33

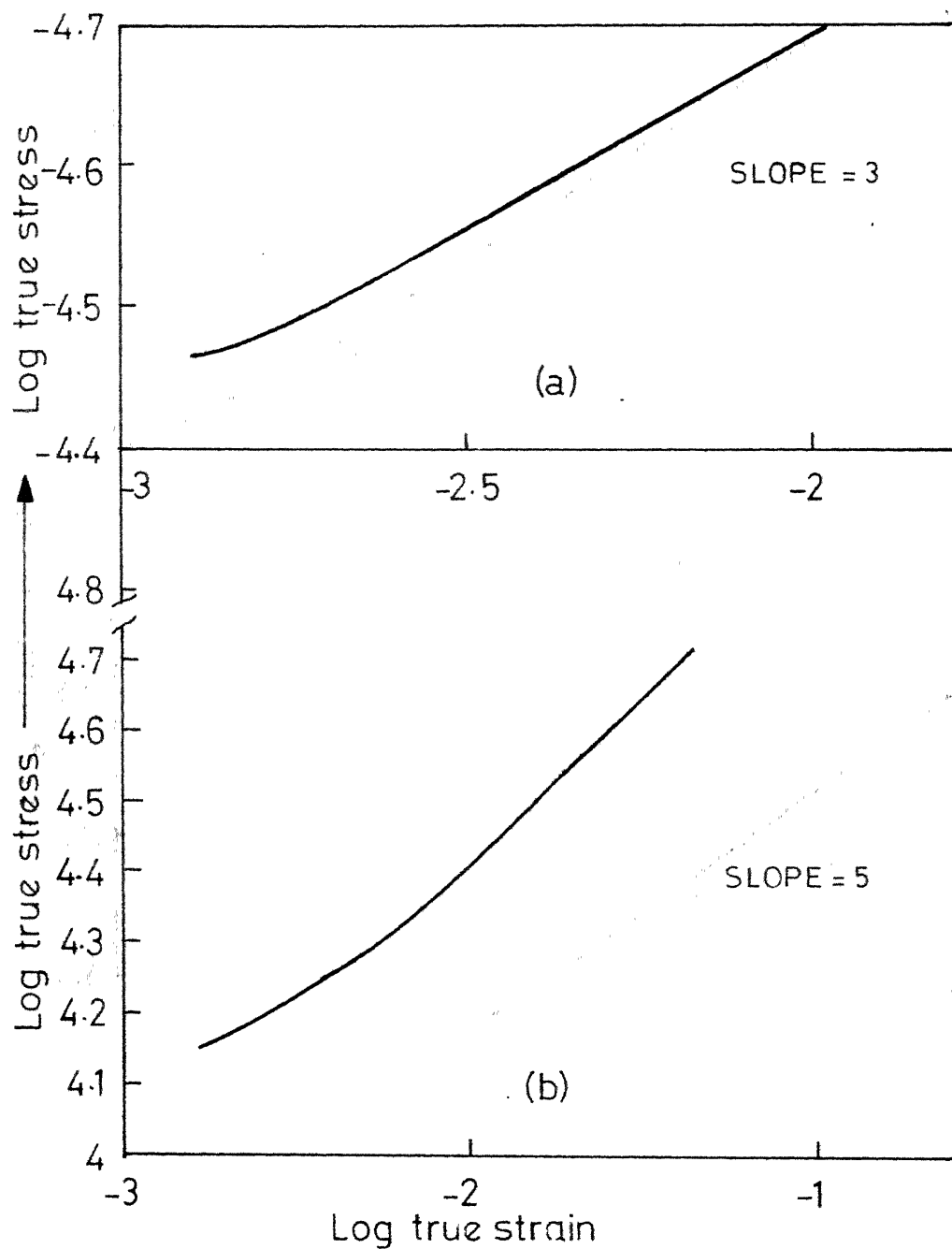


FIG.13. PLOT OF LOG TRUE STRESS VS. LOG TRUE STRAIN.(a) SAMPLE AGED AT 675°C FOR 550 HOURS.(b)SAMPLE AGED AT 675°C FOR 5 HOURS.

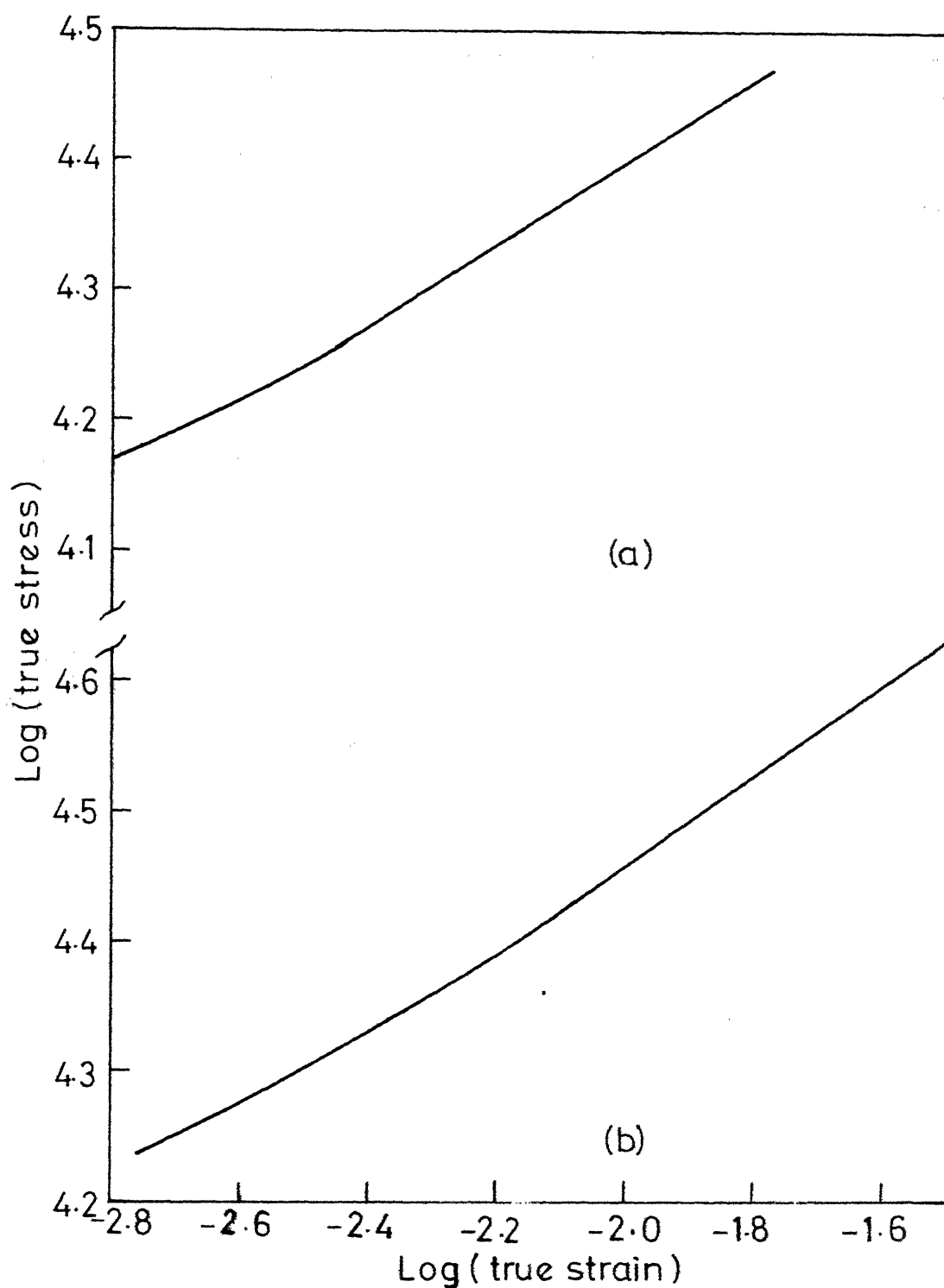


FIG.14. PLOT OF LOG (TRUE STRESS) VS. LOG (TRUE STRAIN)  
(a) SAMPLE AGED AT 725°C FOR 4 HOURS.

\* (b) SAMPLE AGED AT 725°C FOR 8 HOURS.

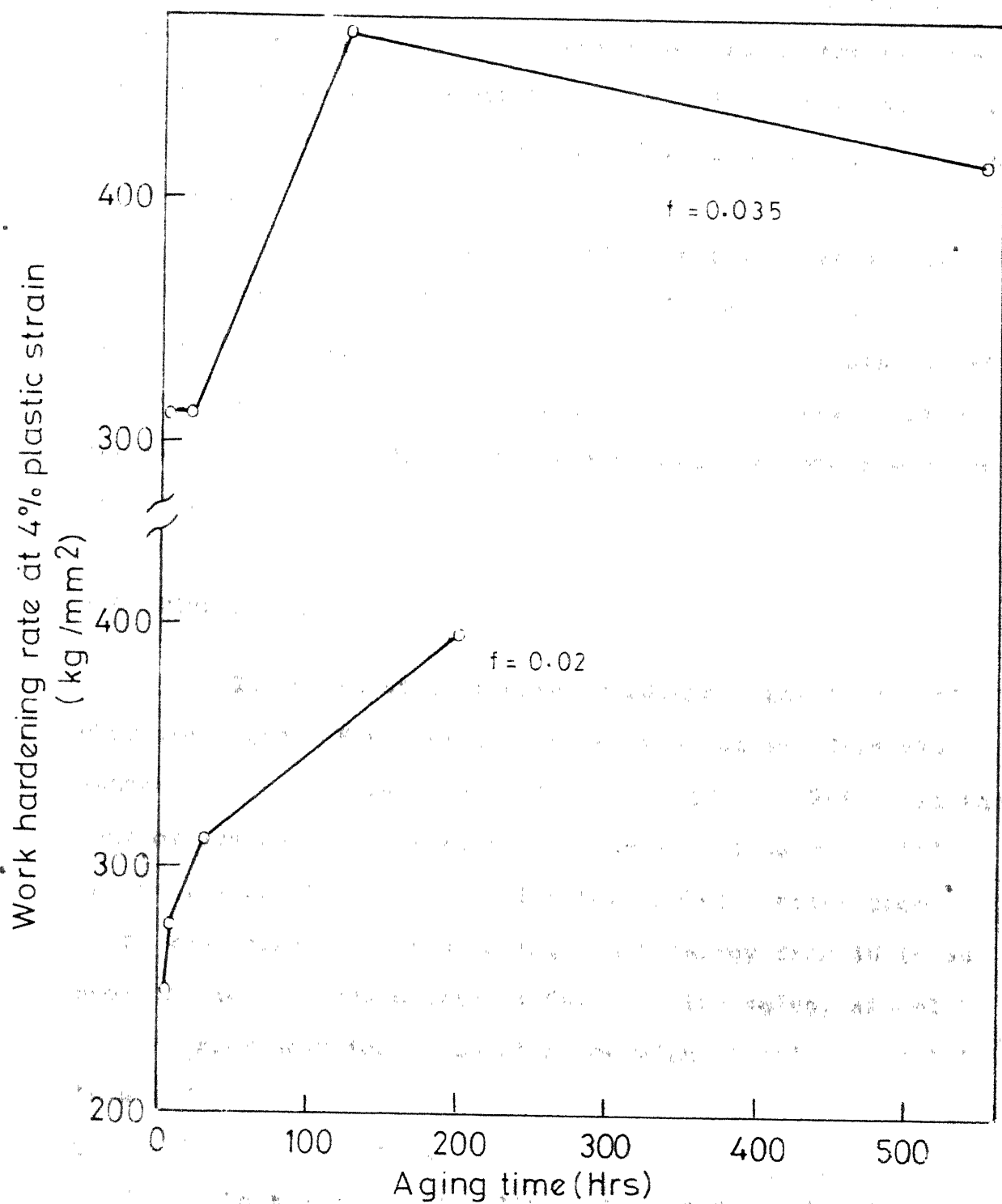


FIG 15 WORK HARDENING RATE AS A FUNCTION OF AGING TIME.

rate cycling tests. The magnitudes of these stresses at different strains obtained by stress relaxation for all samples have been listed in Appendix 3. Using this data Figs. (16-18) have been plotted showing the variation of applied, internal and effective stresses with strain.

Long term stress relaxation data indicates a very gradual rise in effective stress, magnitude of which is much lower than that obtained on the same sample using strain rate cycling. Results on the basis of strain rate cycling are shown in Fig. (19). The detailed calculations are given in Appendix 4.

#### 4.4 Discussion

In the solution treated condition, the deformation characteristics of the single phase material are directly determined by the stacking fault energy (Swann 1963). In the case of austenitic steels, this is dependent on composition and in 15% Cr steels, increasing the nickel content from 9% to 25% increases the stacking fault energy from 10 to 30 ergs/cm<sup>2</sup> (Dulieu and Nutting 1964). During aging, nickel is removed from solution by combination with titanium, resulting in a reduction of stacking fault energy with an increasing volume fraction of Ni<sub>3</sub>Ti.

In the underaged alloys where deformation is by the motion of super-dislocations, the work hardening rate

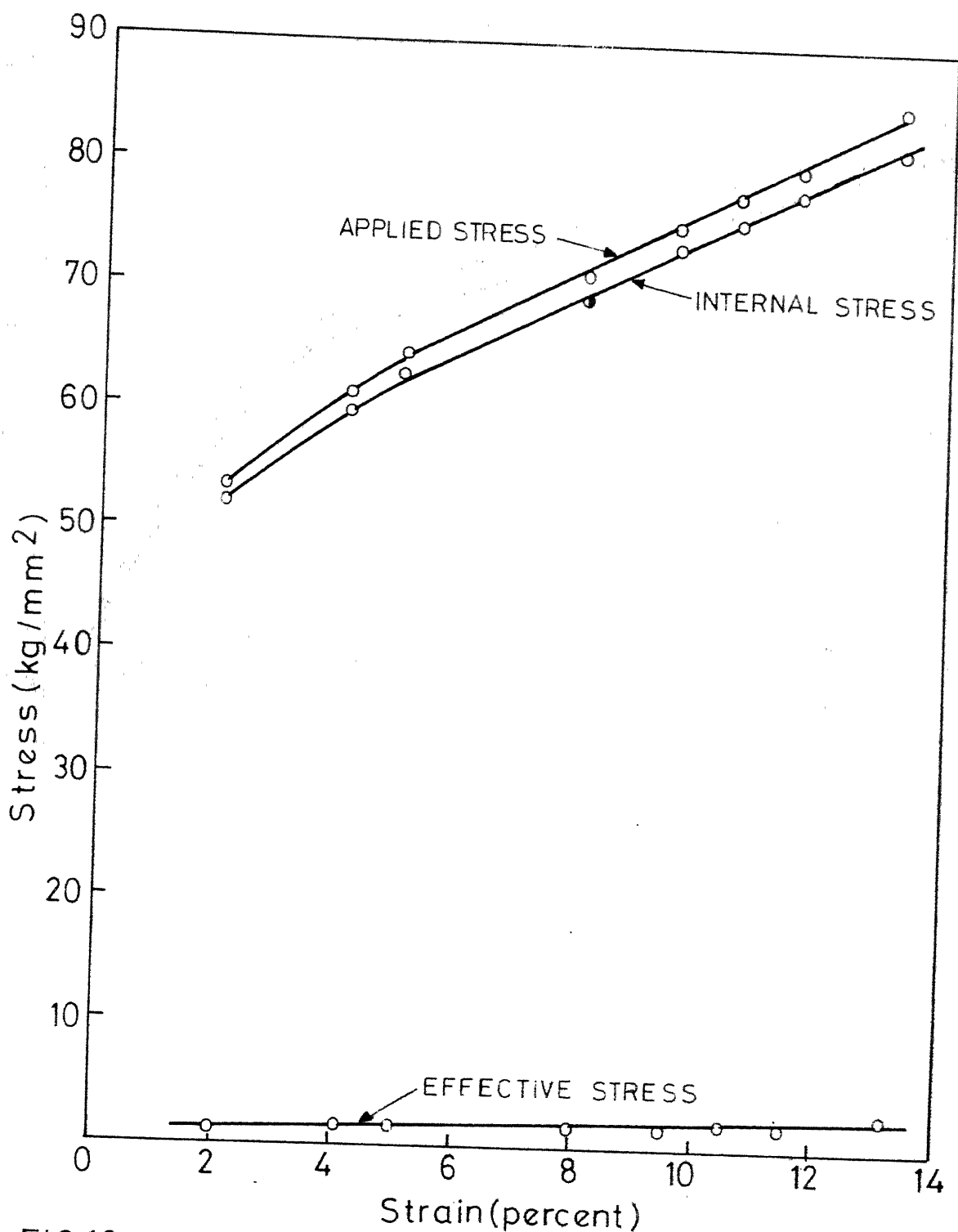


FIG.16. EFFECTIVE AND INTERNAL STRESSES OBTAINED BY STRESS RELAXATION AS A FUNCTION OF THE STRAIN. (Sample aged at 675°C for 20 hours).



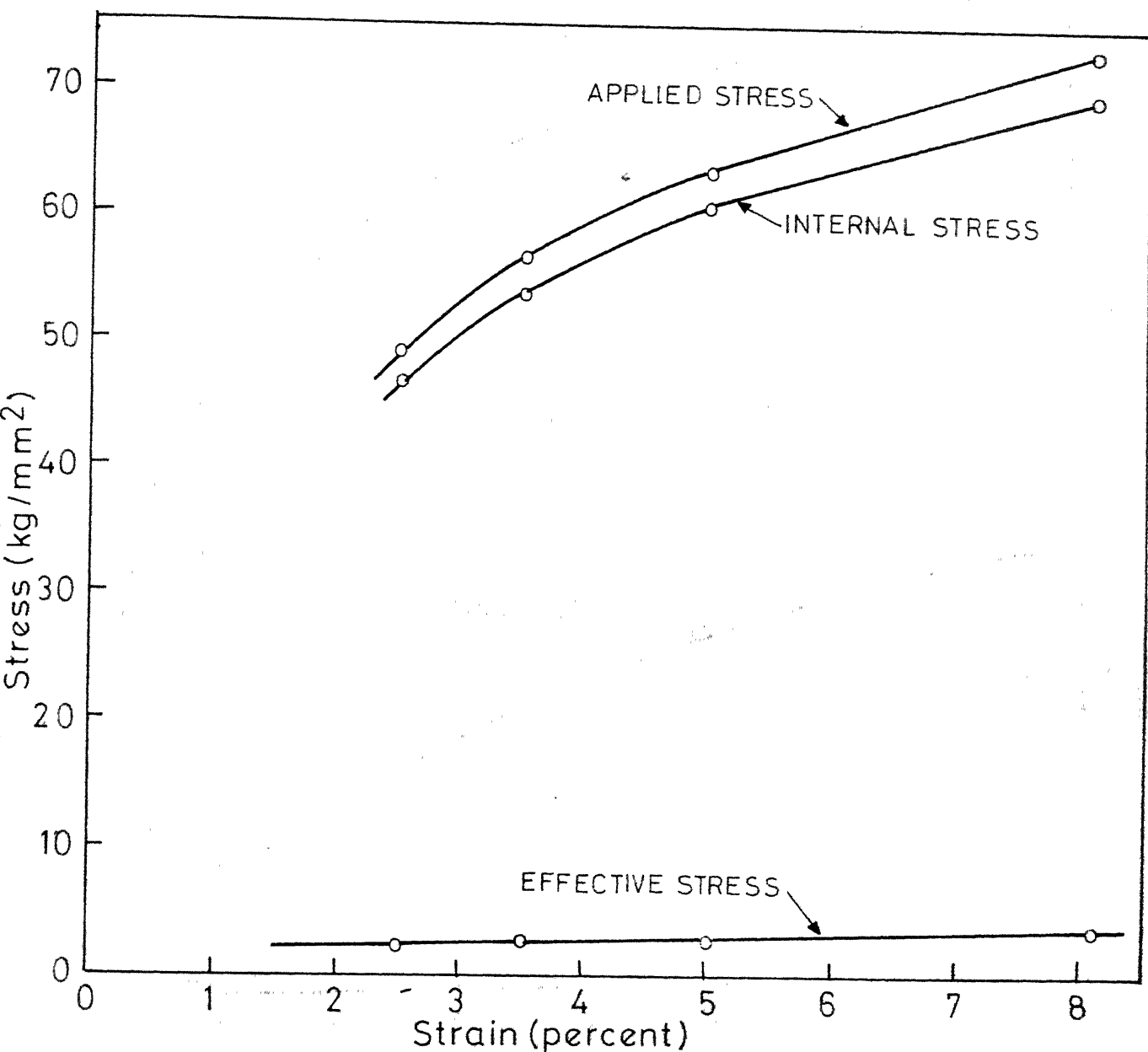


FIG.18. EFFECTIVE AND INTERNAL STRESSES OBTAINED BY STRESS RELAXATION AS A FUNCTION OF THE STRAIN. (Sample aged at 750° C for 1000 hours.)

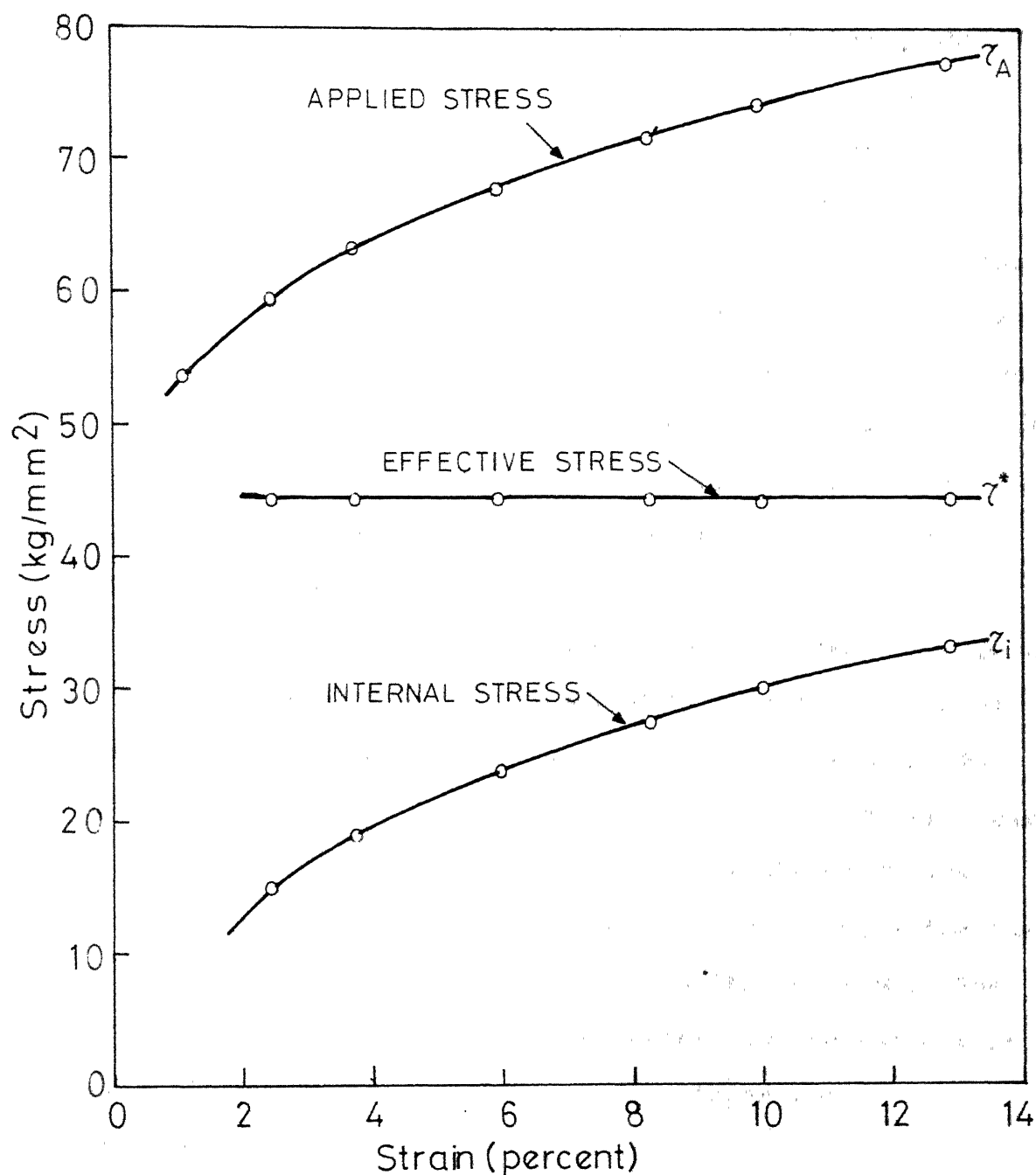


FIG.19. EFFECTIVE AND INTERNAL STRESSES OBTAINED BY STRAIN RATE CYCLING AS A FUNCTION OF THE STRAIN. (Sample aged at 725°C for 30 hours).

can be rationalised by considering the aged precipitate to be a single phase material with a stacking fault energy that is lower than that of the solution treated. The presence of small ordered  $\gamma'$  precipitates increase the stress required for the initial propagation of dislocations due to the anti-phase boundary energy that has to be overcome while cutting the precipitate. Because the moving partials cut the zones, the zones themselves do not make a significant contribution to the work hardening rate. The increase in strength at this stage is mainly a result of restricted cross slip due to the lower effective stacking fault energy and not a direct consequence of the presence of the precipitate.

The increase in the rate of work hardening as aging proceeds corresponds to the change from direct shearing of  $\gamma'$  particles to looping around them. However for looping to occur, the dislocation must not be dissociated. In such cases the leading partial may be held up against the particles and the applied stress is sufficiently high to recombine the partial dislocations before causing looping to occur. The increase in work hardening rate is mainly due to the coarse distribution of  $\gamma'$  particles, which hinder the movement of dislocations.

The results of the stress relaxation and strain rate cycling experiments do not tally. It is suspected that strain rate cycling is not reliable in view of the fact that at large stresses, as encountered in this work, any small

error in measuring the stresses at the two strain rates can cause a large deviation in the results and hence the calculated values of the dislocation velocity stress exponent are unreliable. So basically this method is inadequate at large stresses. It may also be mentioned that the present data on stress relaxation was analysed on the basis of the model of Gupta and Li (1970) unsuccessfully. This may be because while most of the relaxation curves of Gupta and Li showed a deviation from linearity at small relaxation times, this was appreciable in the case of austenitic stainless steels and consequently the slope of the relaxation curve changed appreciably.

## CHAPTER 5

### MOTION OF PARTIAL DISLOCATIONS

#### 5.1 Introduction

In austenitic stainless steels containing  $\gamma'$  particles the deformation depends on the aging kinetics. While at short aging times it has been found that dislocations travel in pairs (Singhal and Martin 1968), after peak hardness loops were observed around the precipitates. Dislocations travel in pairs owing to the cutting of ordered particles (Raynor and Silcock 1970). Gleiter and Hornbogen (1965) developed a theory of the yield stress in alloys containing coherent, stress free ordered particles based on the observation that dislocations glide in pairs. But this theory does not include the details of dislocation motion. In an attempt to overcome this drawback Copley and Kear (1967) proposed a dynamic theory of coherent precipitation hardening. This theory was successful in predicting the yield stress and the observed temperature dependence of yield stress.

In this work an attempt has been made to explain the experimental observation of earlier workers, based on the model of Copley and Kear (1967). The variations of the different parameters related to the theory have been studied. Finally, a new model which overcomes some of the limitations of Copley and Kear's theory has been outlined.

## 5.2 Theory

The dislocation dynamics have been based on the stress dependence of the dislocation velocity ( $v$ ) as given by Gilman (1959)

$$v = v^* \exp (- D/\tau ) \quad (30)$$

where  $v^*$  is a velocity near the shear wave velocity,  $D$  which is a measure of the frictional forces that act on the moving dislocation also termed as the characteristic drag-stress coefficient and  $\tau$  is the stress function. Evaluation of  $\tau$  would aid in calculating the individual velocities of the leading and trailing partials.

Consider the forces acting on the leading (1) and trailing (2) partial dislocations. When the leading moves through the matrix it is acted upon by the following forces:

i) A force due to the applied stress which is  $\sigma b_p m_1 2R_g$ , where  $b_p$  is the Burgers vector of the partial,  $\sigma$  is the applied tensile stress,  $m_1$  is the Schmid factor of the leading partial and  $2R_g$  is the planar interparticle spacing given by eqn. (15).

ii) A force due to the creation of stacking fault  $\gamma_m 2R_g$  where  $\gamma_m$  is the stacking fault energy of the matrix.

iii) A repulsive force  $2R_g c/\Delta x$  due to the trailing dislocation where  $\Delta x$  is the distance between the trailing and leading dislocations and  $c$  is given by (Hirsch and Kelly 1965)

$$c = \frac{G b_p^2 (2 - \nu)}{8 \pi \Delta x (1 - \nu)} \left( 1 - \frac{2 \nu (\cos 2\alpha)}{(2 - \nu)} \right) \quad (31)$$

where  $G$  is the shear modulus,  $\nu$  the Poisson's ratio and  $\alpha$  is the angle the resultant Burger vector makes with the dislocation line.

From this the velocity of the leading partial in the matrix can be given as

$$v(1)_m = v_m^* \exp \left[ \frac{-D_m \cdot 2R_s}{\sigma b_p m_1 \cdot 2R_s - \gamma_m \cdot 2R_s + c/\Delta x \cdot 2R_s} \right] \quad (32)$$

where  $D_m$  is the drag coefficient in the matrix. Similarly the velocity of the trailing dislocation in the matrix can be given as

$$v_2(2)_m = v_m^* \exp \left[ \frac{-D_m \cdot 2R_s}{\sigma b_p m_2 \cdot 2R_s + \gamma_m \cdot 2R_s - 2R_s \cdot c/\Delta x} \right] \quad (33)$$

where  $m_2$  is the Schmid factor of the trailing partial dislocation.

As the leading partial enters the precipitate its motion is impeded since it must create anti-phase boundary. Consequently the forces now acting on the leading partial in the precipitate are;

- i) A force due to the applied stress  $\sigma b_p m_1 \cdot 2R_s$ .
- ii) A force due to the creation of stacking faults in the precipitate  $\gamma_p \cdot S_1$  where  $S_1$  is the length of the dislocation inside the precipitate at any instant,  $\gamma_p$  is the stacking fault energy of the precipitate.

iii) A force due to the creation of stacking fault in the matrix  $\gamma_m \cdot (2R_s - S_1)$ .

iv) A repulsive force  $2R_s \cdot c / \Delta x$ .

v) A force due to the anti-phase boundary  $\gamma_{APB} \cdot S_1$  where  $\gamma_{APB}$  is the anti-phase boundary energy. The velocity in the precipitate is thus given by

$$v(1)_p = v_p^* \exp \left[ \frac{-D_p \cdot S_1 - D_m(2R_s - S_1)}{\sigma_b p m_1 \cdot 2R_s - \gamma_m(2R_s - S_1) - \gamma_p S_1 - \gamma_{APB} \cdot S_1 + 2R_s \cdot c / \Delta x} \right] \quad (34)$$

where  $D_p$  is the drag coefficient of the precipitate. Similarly, the velocity of the trailing in the precipitate is given by

$$v(2)_p = v_p^* \exp \left[ \frac{-D_p \cdot S_2 - D_m(2R_s - S_2)}{\sigma_b p m_2 \cdot 2R_s + \gamma_p \cdot S_2 + \gamma_m(2R_s - S_1) - 2R_s \cdot c / \Delta x} \right] \quad (35)$$

where  $S_2$  is the segment of the trailing partial in the precipitate. The trailing partial neither creates nor annihilates the antiphase boundary.

### 5.3 Results

On the basis of these equations numerical values were inserted in eqns. (31)-(35) to evaluate the velocities of the leading and trailing partials. The velocities and separations between partials were calculated on an IBM 7044 computer. The positions of the leading and trailing partials were obtained for every  $1 A^\circ$  movement of the leading.



Since the equilibrium structure for  $\text{Ni}_3\text{Ti}$  is  $\text{DO}_{24}$ , it is not possible to prepare  $\text{Ni}_3\text{Ti}$  with ordered  $\text{Li}_2$  structure. Therefore, the drag coefficient of the precipitate  $D_p$ , is taken to be the same for  $\text{Ni}_3\text{TiAl}$  (Kear and Piercey 1965). The following values of different parameters were used for calculations;

$$\begin{aligned} 2R_s &= 300 \text{ \AA}, \quad 2r_s = 100 \text{ \AA}, \quad b_p = 1.45 \text{ \AA}, \\ \sigma &= 80.5 \text{ kg/mm}^2, \quad \gamma_{\text{APB}} = 280 \text{ ergs/cm}^2, \quad \gamma_m = 15 \text{ ergs/cm}^2 \\ c &= 10^{-5} \text{ ergs}, \quad \Delta x = 70 \text{ \AA}, \quad v_p^* = v_m^* = 2.52 \times 10^5 \text{ cm/sec} \\ m_1 &= 0.47, \quad m_2 = 0.24 \end{aligned}$$

This data was used for a steel in which dislocation partials moved in pairs (Wilson and Pickering 1969). The plot of dislocation velocity of leading and partial dislocations as a function of the position of dislocations is qualitatively shown in Fig. (20). As the leading dislocation moves through the matrix, separation between the partials increases. Hence the repulsive force decreases resulting in a slowing down of the leading partial dislocation while the trailing experiences an acceleration. As soon as the leading partial enters the precipitate, its velocity drops sharply due to the creation of an anti-phase boundary as also due to the higher drag coefficient of the precipitate. Due to the reduced speed of the leading partial the separation between them decreases and as a result the repulsive force on the trailing now begins to increase. Similarly, when the trailing partial enters the precipitate, its velocity also decreases rapidly an account of the higher drag coefficient

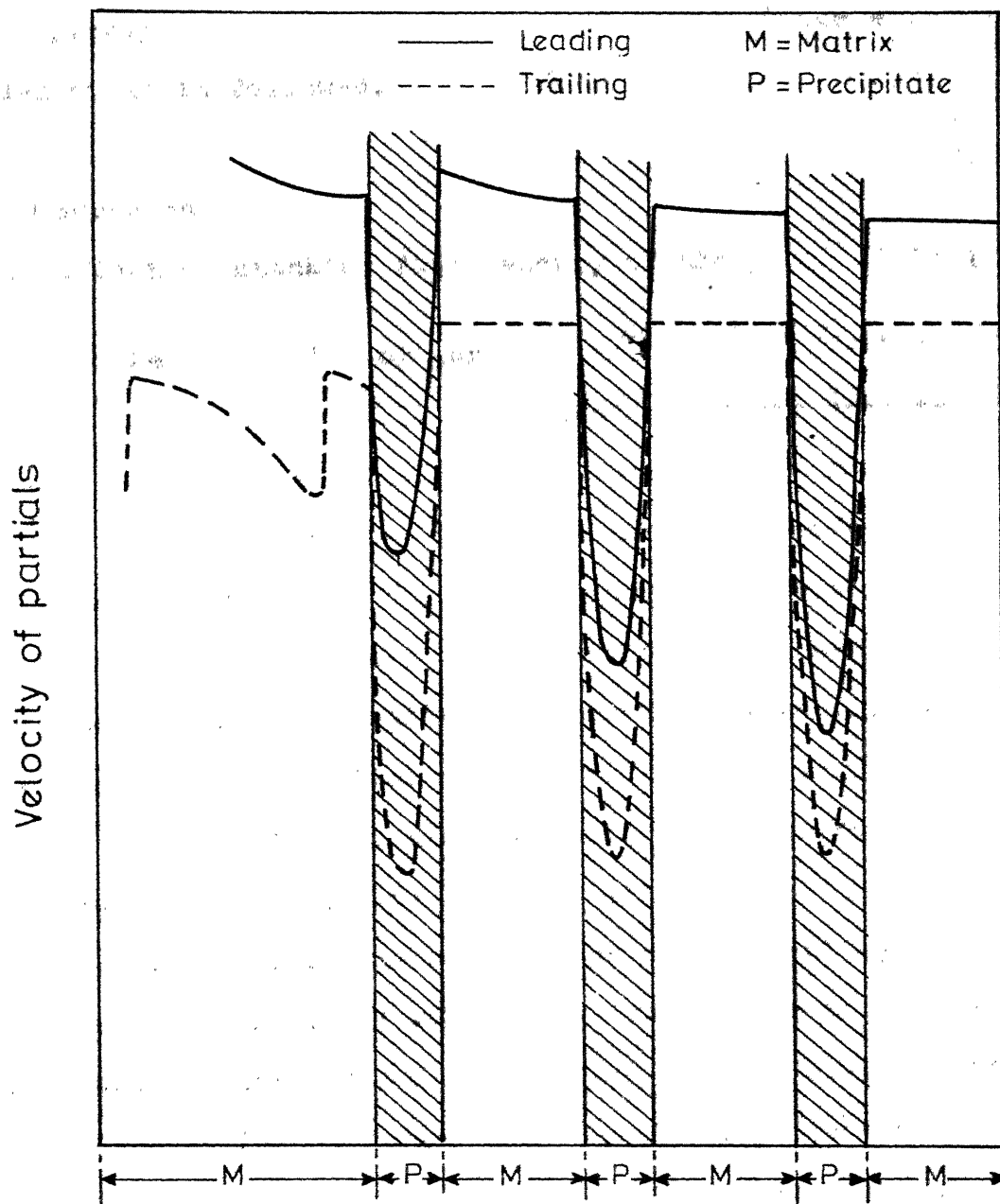


FIG.20 MOTION OF PARTIAL DISLOCATIONS MOVING IN A MATRIX CONTAINING PRECIPITATES.

of the precipitate. Once both leave the precipitate a similar cycle is followed.

## 5.4 Discussion

### 5.4.1 Effect of stacking fault energy of the precipitate ( $\gamma_p$ ):

The separation of partials for different values of  $\gamma_p$  is shown in Fig. (21). A computer program used to evaluate the velocities is listed in Appendix 5. The separation keeps increasing for values of  $\gamma_p$  below - 50 ergs/cm<sup>2</sup>. But for higher values of  $\gamma_p$  the separation decreases. This is mainly a result of a negative stacking fault energy which tends to aid the leading - for more negative values of  $\gamma_p$  while it assists motion of the trailing for larger values. Such large separations were in fact observed by Wilson and Pickering (1969) in their alloys.

Similar data was used on the alloys used by Singhal and Martin (1968), the volume fraction in this case being 0.02. In this case  $\sigma = 37 \text{ kg/mm}^2$  and  $\gamma_m = 20 \text{ ergs/cm}^2$ . This is because in the former case when volume fraction was 0.1 then  $\gamma_m = 15 \text{ ergs/cm}^2$  only because a lot of nickel has been taken out to form  $\text{Ni}_3\text{Ti}$  and hence the matrix has lesser nickel and consequently a lower  $\gamma_m$ . In this case no dissociation was observed for  $\gamma_p = - 35 \text{ ergs/cm}^2$  as shown in Fig. (22). This is in complete agreement with the experimental findings (Singhal and Martin 1968).

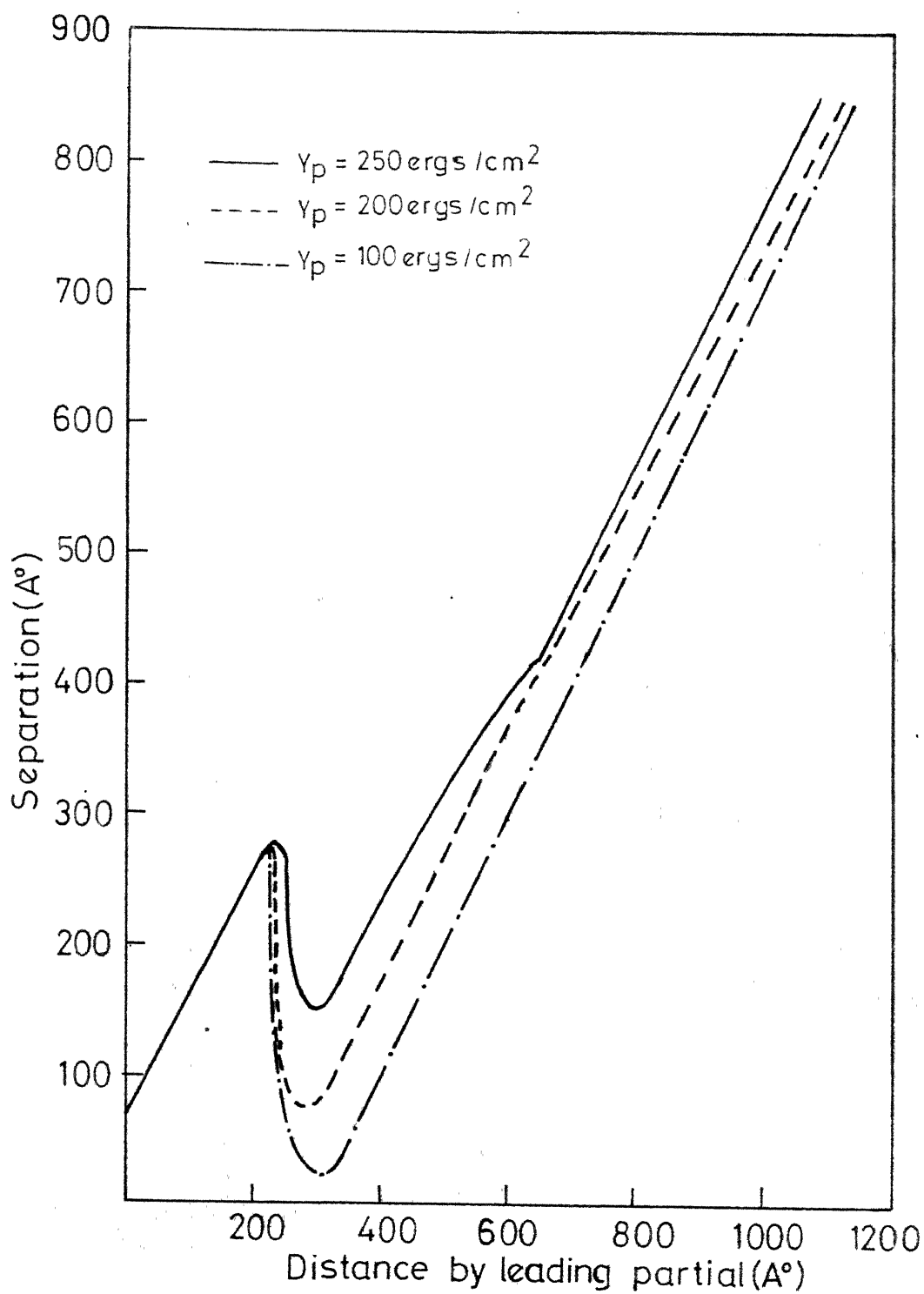


FIG. 21. EFFECT OF STACKING FAULT ENERGY OF THE PRECIPITATE ON DISLOCATION SPACING FOR VOLUME FRACTION OF 0.1.

#### 5.4.2 Effect of orientation:

Orientation has a marked effect on the dislocation velocities. The separation is greatly influenced due to changes in Schmid factor of the leading and trailing partial dislocations. The Schmid factors for different orientations are shown in Table 5 (Copley and Kear 1968).

TABLE 5

Schmid factors for the leading and trailing partials for different orientations

Orientation	$m_1$	$m_2$
[101]	.47	.24
[001]	.24	.47
[111]	.31	.16
[113]	.4	.4

This implies that while in [101] direction the effect of the applied stress on the leading is twice that on the trailing whereas in [001] is vice versa. Consequently, the separation in [101] direction increases continuously while along [001] dissociation does not occur. In the [111] direction the ratio of the Schmid factors is the same as that in [101] and shows a similar effect as in [101]. The only difference is that the time now involved in crossing the precipitates is much greater now. In the [113] direction where the Schmid factors are equal it is found that the 'steady state' sets in.

This implies that after crossing one or two particles the average separation does not change. This shows that once dissociation starts it may not necessarily go on and on, but may maintain an average separation. These effects are illustrated in Fig. (23).

#### 5.4.3 Effect of stacking fault energy of the matrix $\gamma_m$ :

The stacking fault energy of the matrix has been given as 15 ergs/cm<sup>2</sup> (Dulieu and Nutting 1964, Thomas 1963). Increasing  $\gamma_m$  to 20 ergs/cm<sup>2</sup> decreases the velocity of the leading, but increases the velocity of the trailing while for lower values of  $\gamma_m$  the separation is larger than that at 15 ergs/cm<sup>2</sup> Fig. (24). This is because less resistance is offered to the movement of the leading partial while at the same time the trailing moves slowly, since the energy of the fault which it eliminates is much lesser now.

#### 5.4.4 Effect of antiphase boundary energy $\gamma_{APB}$ :

The effect of antiphase boundary energies on separation of partial dislocations is shown in Fig. (25). The higher the value of  $\gamma_{APB}$ , the more the resistance is offered to the passage of the leading partial, thereby decreasing the interparticle spacing. The velocity of the trailing partial remains unaffected since it neither creates nor destroys an antiphase boundary.

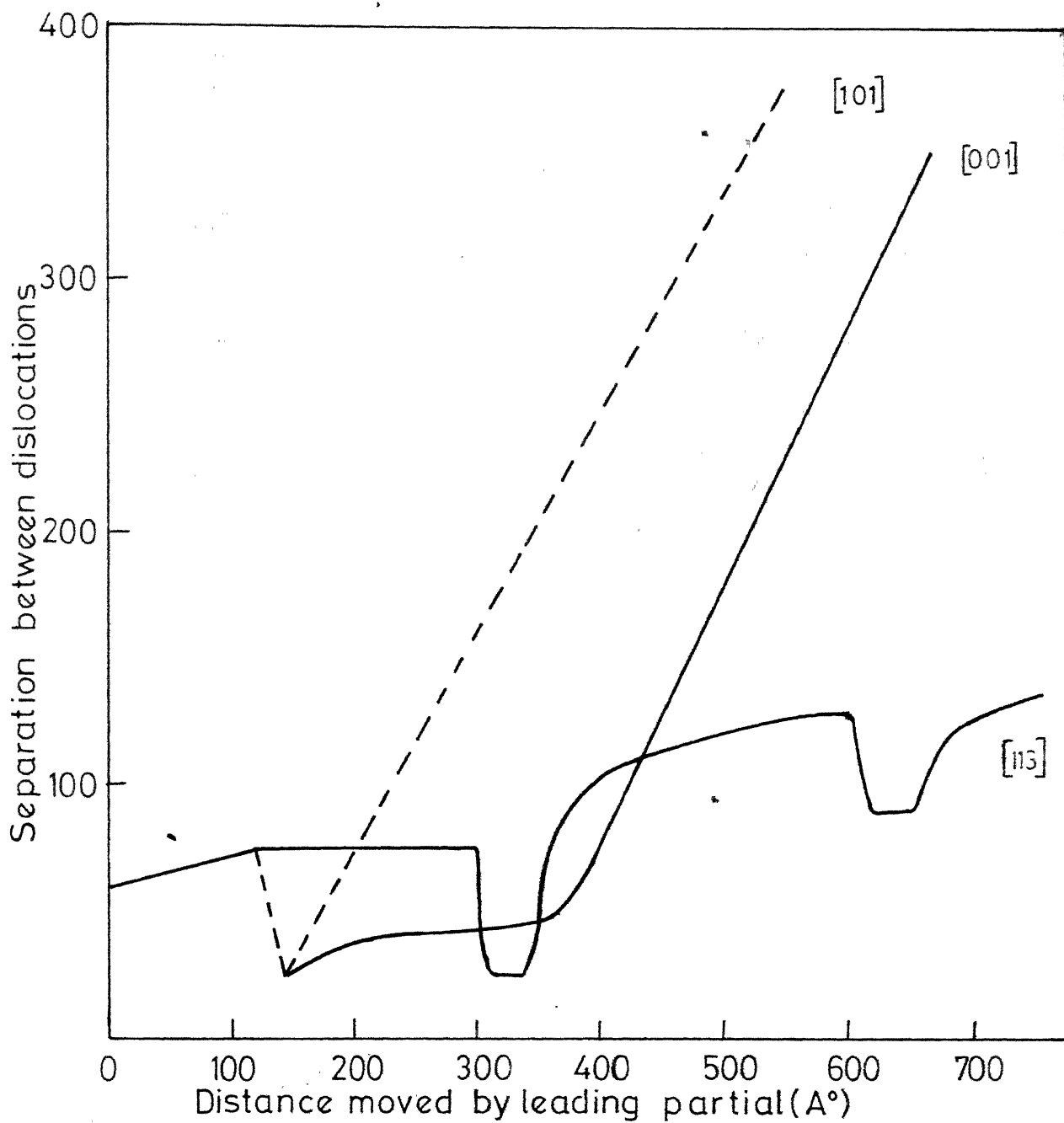


FIG.23. EFFECT OF ORIENTATION ON DISLOCATION SPACING.

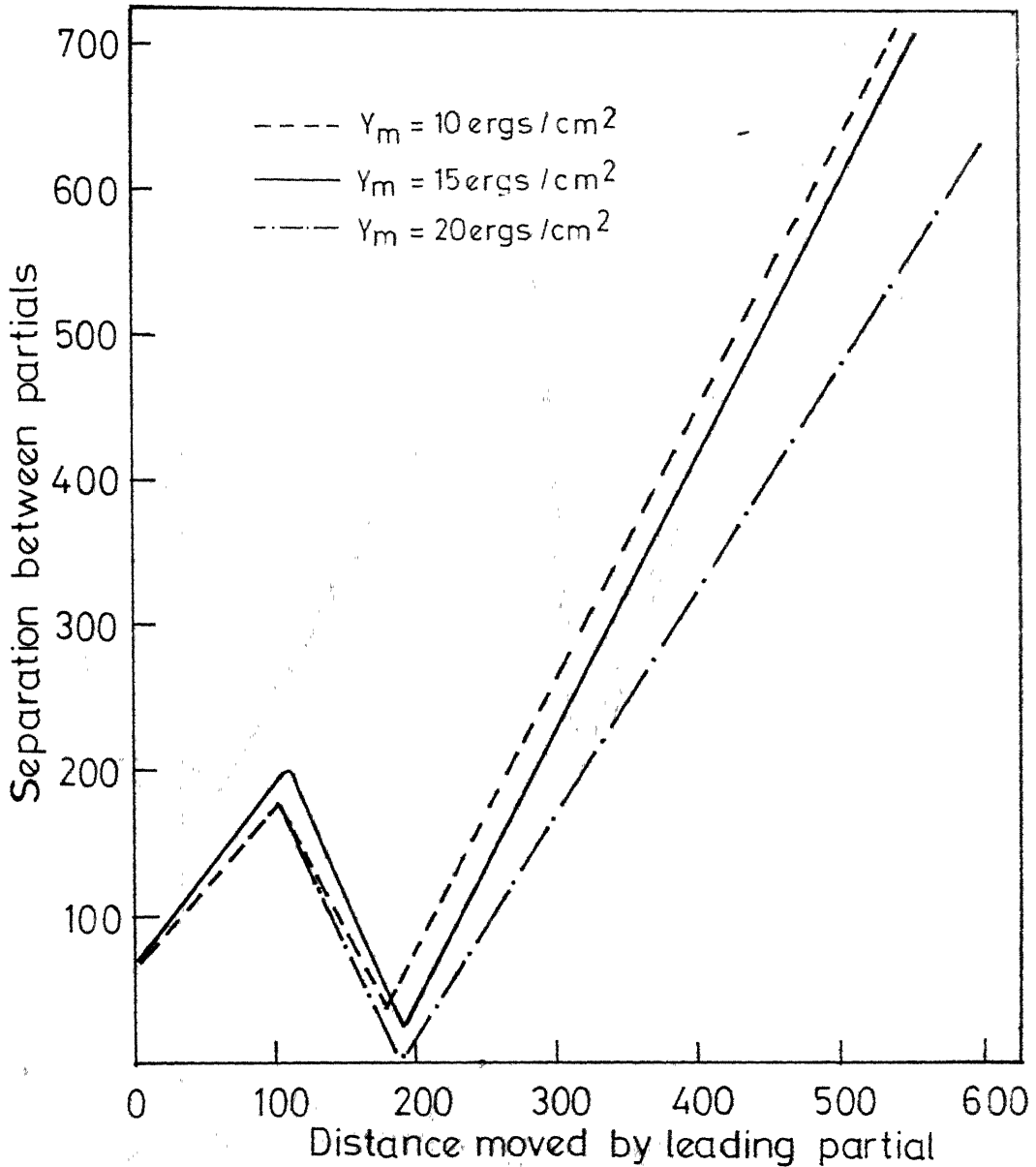


FIG.24. EFFECT OF STACKING FAULT ENERGY OF THE MATRIX ON SEPARATION BETWEEN PARTIALS ( $Y_p = -60 \text{ ergs/cm}^2$ )



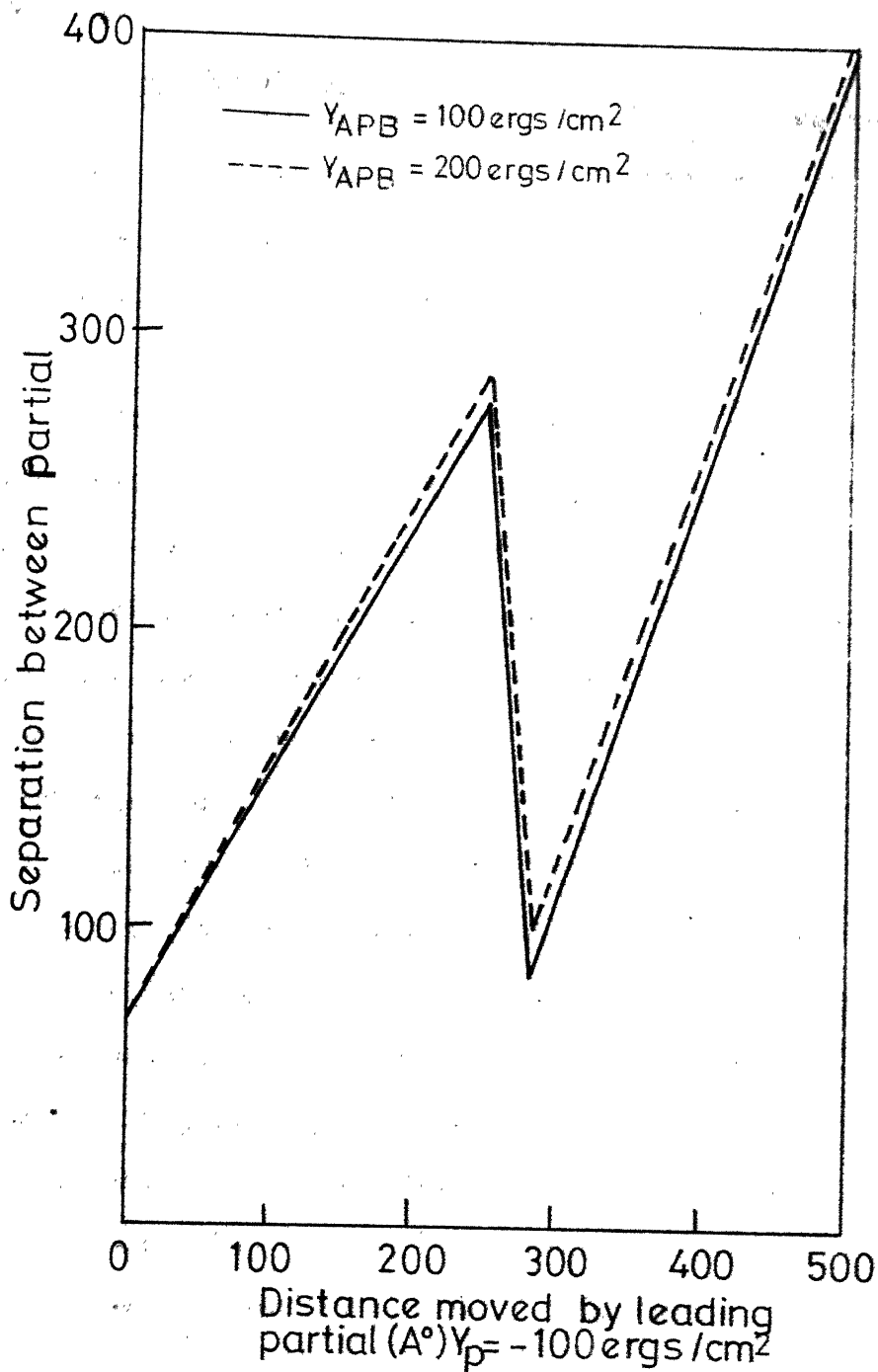


FIG. 25. EFFECT OF THE ANTIPHASE BOUNDARY ENERGY OF PRECIPITATED  $D_p$  ON DISLOCATION SPACING ( $Y_p = -60 \text{ ergs/cm}^2$ )

#### 5.4.5 Effect of drag coefficient ( $D_p$ ) of the precipitate:

Unlike  $\gamma_m$ ,  $\gamma_p$  and  $\gamma_{APB}$ , an increase in the drag coefficient of the precipitate reduces the velocity of both partials as in Fig. (26). Hence its effect is not very pronounced. A similar effect would be seen by increasing the drag coefficient of the matrix  $D_m$ .

Thus, this approach satisfactorily explains experimental observations of Singhal and Martin (1968), Singhal (1968) and Wilson and Pickering (1969). Like the static model of Gleiter and Hornbogen (1965) the dynamic theory also predicts complete separation between partials in steel for negative values of  $\gamma_p$ . Orientation effects are such that only some of the dislocations would be widely spaced. Another interesting feature is the stabilisation of the separation after some dissociation has taken place.

While in the above model of Copley and Kear (1967), the equations have been used assuming the dislocations to be perfectly straight, ~~but~~ this is not usually the case. In order to overcome this drawback a modified version of the dynamic theory which accounts for the curvature of the dislocations has been proposed in this work.

#### 5.5 Present Model

As soon as the dislocation reaches the precipitate, the segment in contact with the precipitate assumes a curvature as that of the precipitate while the free segment

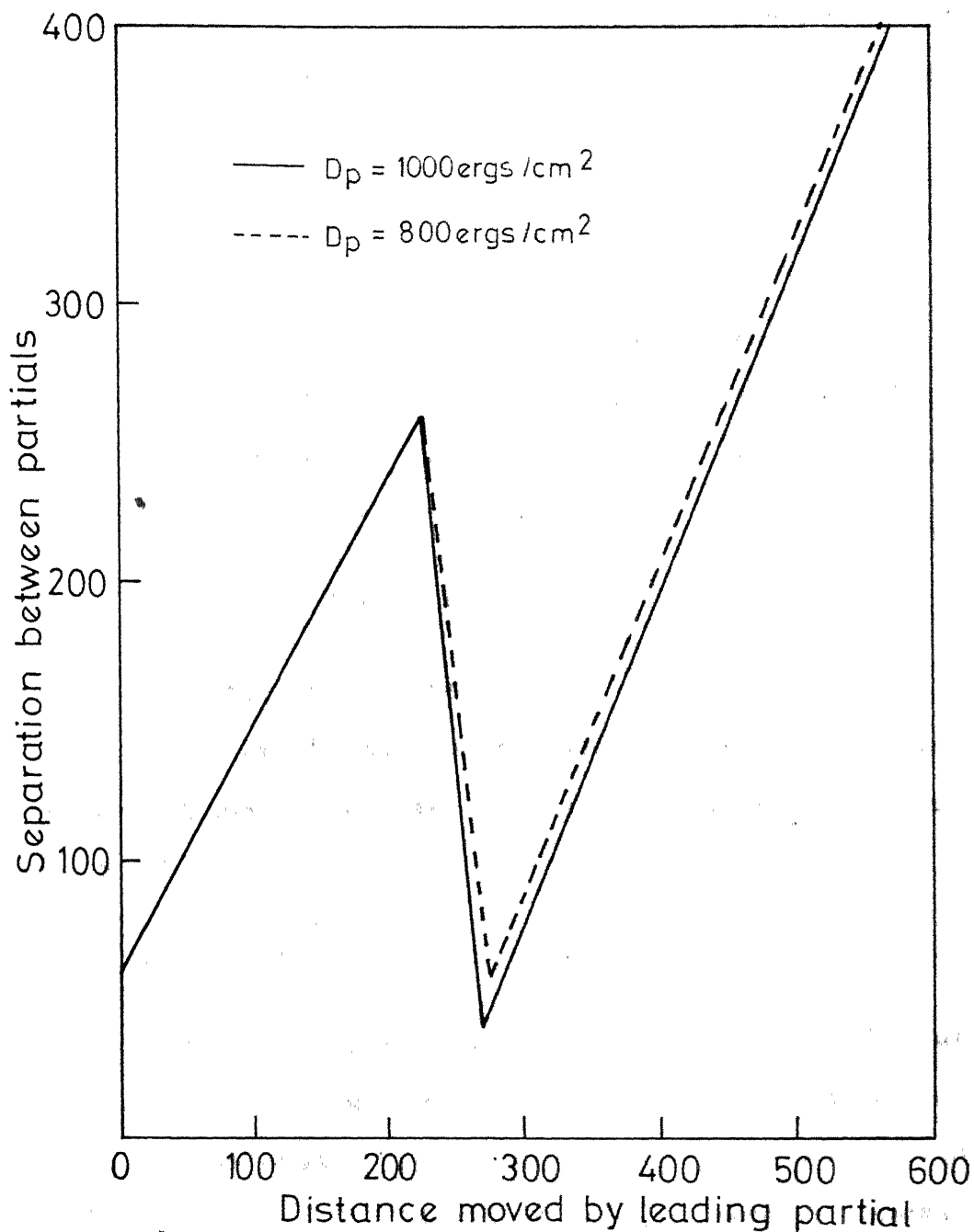


FIG. 26. EFFECT OF DRAG COEFFICIENT OF THE PRECIPITATE  $D_p$  ON SEPARATION BETWEEN PARTIALS ( $\gamma_p = -100 \text{ ergs/cm}^2$ )

begins to bow as shown in Fig. (27). The average inter-particle spacing for a flexible dislocation line of Burgers vector  $b_p$  is given by (Singhal 1970)

$$2R'_s = 2 \left[ \frac{2TR_V^2}{\tau b_p} \right]^{1/3} R_s / \left[ \left( \frac{2TR_V^2}{\tau b_p} \right) + R_s \right] \quad (36)$$

where  $T$  is the line tension of the dislocation,  $\tau$  the applied shear stress,  $2R'_s$  is the mean planar particle separation given by eq. (15),  $2R_V$  is the mean interparticle spacing given by (Pott and Nabarro 1940)

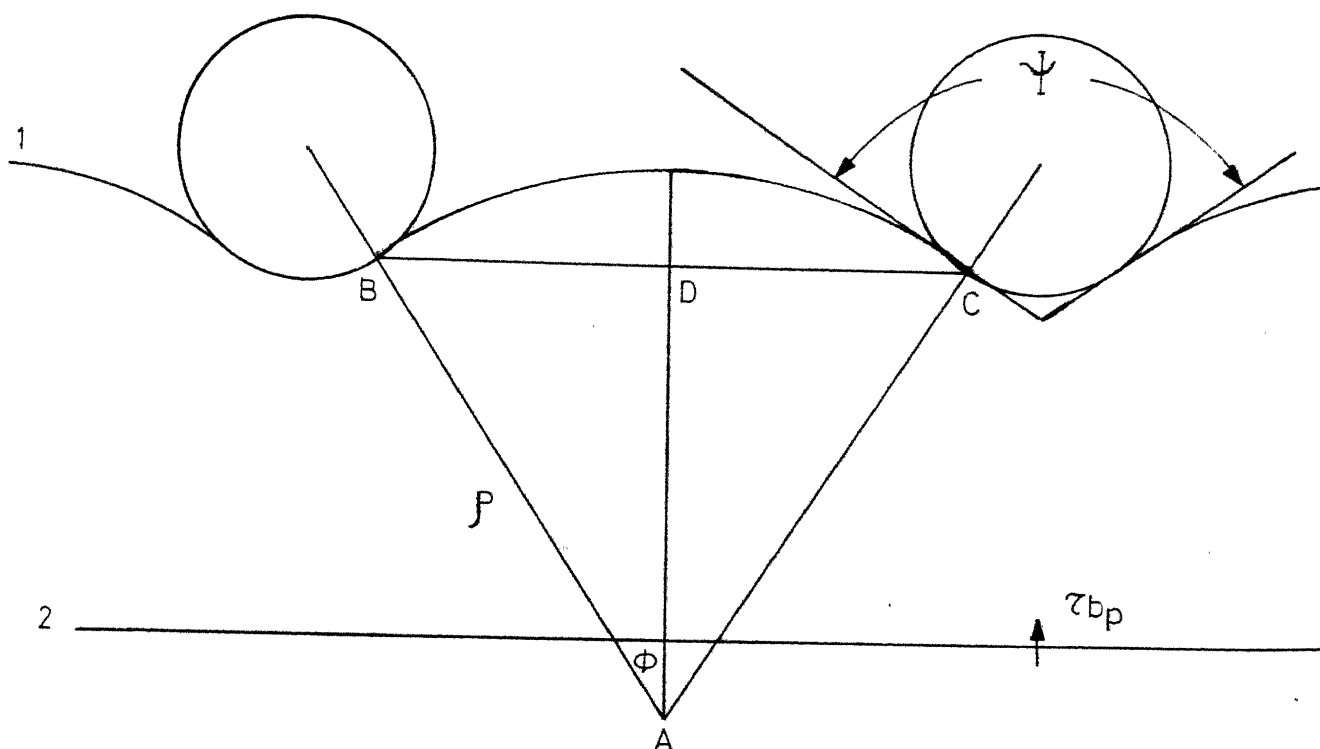
$$2R_V = \left( \frac{\pi}{6f} \right)^{1/3} r_V \quad (37)$$

where  $r_V$  and  $r_s$  are related by eqn. (29).

$\psi$  which is the angle formed by the two tangents from the points of contact with the precipitate is given by (Guyot 1971)

$$\cos \psi/2 = \frac{b_p \cdot 2R'_s \tau}{2T} \left( 1 - \frac{b_p \tau}{\gamma_{APB}} \right) \quad (38)$$

where  $R'_s$  is given by eqn. (36) and  $\tau$  is the applied stress. Knowing  $\psi$ , the length of the arc of contact can be estimated. From  $\psi$ , the angle  $\phi$  at A may also be obtained. Using  $\phi/2$  and knowing the length  $BC = 2R'_s$  - constant length along the precipitate, the length AB is calculated. AB is now the radius of curvature of the free segment and since  $\phi$  is known the length of the free segment is also obtained.



- $\tau$ : APPLIED SHEAR STRESS,  
 $b_p$ : BURGERS VECTOR OF PARTIAL.  
 $P$ : RADIUS OF CURVATURE OF FREE SEGMENT.  
 1: LEADING PARTIAL,  
 2: TRAILING PARTIAL.

FIG. 27. BOWING OF PARTIAL DISLOCATION.

The forces on both the free segment and that in contact with precipitate are evaluated separately. The velocities are

i) velocity of the leading partial in contact with precipitate  $v(1)_p$

$$v(1)_p = v_p^* \exp \left[ \frac{-D_p}{\tau b_p - \gamma_p - \gamma_{APB} + L_t b_p + c/\Delta x} \right] \quad (39)$$

ii) velocity of free segment of the leading partial

$$v(1)_m = v_m^* \exp \left[ \frac{-D_m}{\tau b_p - \gamma_m - \sigma_s b_p + c/\Delta x} \right] \quad (40)$$

iii) velocity of the trailing in the matrix

$$v(2)_m = v_m^* \exp \left[ \frac{-D_m}{\tau b_p + \gamma_m - c/\Delta x} \right] \quad (41)$$

where  $\sigma_s$  is the self stress given by

$$\sigma_s = \frac{Gb}{4\pi r'} \left[ \frac{1 - 2\nu}{1 - \nu} \right] \ln \frac{2R'_s}{b} \quad (42)$$

$r'$  being the radius of curvature of the free segment.

The trailing partial is given an increment and at each position the velocities of both segments of the leading partial are calculated and hence their position after a fixed time interval. A better estimate may be obtained by multiplying each of the factors in the velocity equation by the length over which it acts. One set of calculations are shown in Appendix 6.

## CHAPTER 6

### CREEP DEFORMATION

#### 6.1 Introduction

Creep is defined as the plastic flow under a constant stress. Creep may be transient or continuous depending on the stress and temperature. Creep of dispersion strengthened materials has not been very well established, especially the variation of creep rate with particle size. In this work it has been attempted to extend the yield model approach described in Chapter 3 to assess creep rates as a function of particle size during the later stages of aging of an austenitic stainless steel containing  $\gamma'$  particles.

#### 6.2 Review

As crystalline materials work harden in the process of deformation, continuing deformation under constant stress implies recovery. The creep rate then results from a balance of simultaneous work hardening and recovery processes. Theories of creep deformation at elevated temperatures can be divided into two groups:

1. Recovery creep theories - which say that creep takes place because strain hardening is continuously annealed out by recovery.

2. Slip theories - which neglect recovery and apply reaction rate theory to some slip process that is supposed to be the rate controlling event.

### 6.2.1 Recovery creep theory:

Recovery creep theories were postulated years back by Bailey (1926), Orowan (1946) and later by Weertman (1957). In the steady state creep condition reached eventually at high temperature, according to the recovery theory strain hardening must be exactly balanced by recovery to maintain a constant mechanical state in which the flow stress  $\sigma$  remains invariant with time  $t$ , so that

$$d\sigma = \left(\frac{\partial \sigma}{\partial \varepsilon}\right) d\varepsilon + \left(\frac{\partial \sigma}{\partial t}\right) dt = 0 \quad (43)$$

$$\text{or } \frac{d\varepsilon}{dt} = \dot{\varepsilon} = \frac{r}{h} \quad (44)$$

where  $r = \left(-\frac{\partial \sigma}{\partial t}\right)$  is the rate of recovery and  $h = \left(-\frac{\partial \sigma}{\partial \varepsilon}\right)$  is the coefficient of strain hardening,  $\varepsilon$  being the strain.

Equation (44) could be tested over a range of conditions by making measurements of  $\dot{\varepsilon}$ ,  $r$  and  $h$ . The works of Cottrell and Aytakin (1950), and Davies, Davies and Wilshire (1965) seem to fit this theory. McLean and Hale (1961), Ishida and McLean (1967) and McLean (1966) have shown that the above is a very general relationship. These theories, however, are not generally applicable to high strength dispersion hardened materials. These theories fail to account for the high stress dependence of the recovery and creep rates (Wilcox and Cluer 1966; Wilcox et al. 1967). The theories



of McLean assume that the dislocations formed during creep exist on a three dimensional net work and the growth of such a net work, essentially by climb of dislocations, constitutes the recovery process (Weertman 1957). By using an impedance factor Lagneborg (1968) was able to account for the creep behaviour of particle hardened material by using a modified recovery theory. Gibbons work on Ni/Cr/Al alloys at constant stress shows that there is a proportional relation between creep rate and recovery rate for materials with different titanium content and dispersions of  $\gamma'$  precipitates. The results of niobium stabilised austenitic stainless steels (William and McLaughlin 1970) also confirm the recovery creep model. But the fact that dislocation network has not been microscopically examined in crept specimens, more or less rules out recovery creep model in  $\gamma'$  precipitation hardened steels.

#### 6.2.2 Slip theories:

The diffusion creep approach (reviewed by Garofalo 1965, Kennedy 1963, Finne and Heller 1959, Sherby and Burke 1967) established that self diffusion is the ultimate rate controlling process in the steady state creep. This was a result of the activation energy of creep and activation energy of self diffusion being nearly equal. Appreciable

creep rates can be produced in fine grained material by a diffusional mass transport of atoms from one grain boundary to another. This phenomenon is the Nabarro-Herring creep (Nabarro 1948, Herring 1950). On this basis it was suggested that creep rate is proportional to the applied stress which does not generally hold good for precipitation hardened alloys.

In the presence of solute, dislocation motion is hindered considerably. Creep at high temperature but low stresses has been explained by the solute drag. This approach due to Friedel (1964), predicts an increasing creep rate with aging time.

Barret and Nix (1965), suggested that creep was controlled by the drag of jogs in screw dislocations. But this also was not applied to  $\gamma$  ' precipitation hardened steels since electron microscopic observations do not reveal the presence of jogs.

Ansell and Weertman (1959) using a dislocation climb model suggested that mobile dislocations climb over particles and are annihilated by dislocations of opposite sign on neighbouring parallel slip planes. At low stress the theory predicts an inverse relationship between creep rate and particle radius. While dislocation loops surround the precipitate, the rate controlling process is the climb of these loops. Thus at high stresses the creep rate increases with particle size.

McLean (1962) predicted the variation of creep rate with aging period in precipitation hardened alloys. This would depend on the nature of interaction of the dislocation with the precipitate which it encounters during glide. This gives rise to four distinct cases viz.;

i) if the particle size and hence inter-particle spacing is large enough to enable easy loop formation, then the creep behaviour is similar to that predicted by Ansell and Weertman (1959).

ii) at small particle sizes it is possible that the dislocation can push the particles ahead. This causes a vacancy imbalance at the rear and front edge of the particle. This predicts that creep rate is proportional to  $1/r^2$ .

iii) if the dislocations can cut through the precipitate, the resistance offered to cutting is proportional to the dislocation length in contact with precipitate which is inversely proportional to the separation of particles and hence the creep rate proportional to  $r/d$  (where  $d$  is the glide distance) which is a constant.

iv) if at a particle size when both cutting and looping cannot occur, then dislocation climb may occur. Since it has to climb a length  $r$ , and then glide over a distance  $d$ , creep rate is proportional to  $d/r$ , which is a constant.

These mechanisms suggest that the creep rate first decreases, remains constant and then increases with aging time. This has been verified experimentally by Singhal and Martin (1967).

In the present work it has been attempted to qualitatively propose a model to assess creep rates in materials where looping around precipitates occur.

### 6.3 Present Model

The basic assumption of this model is that the tensile stress is equal to twice the critical stress to cause bowing.

Case (i). When only one loop forms

$$\tau_A = \tau_{C_1} = \frac{Gb}{2\pi L} \ln \frac{L}{r_0} \quad (45)$$

where  $L = 2R_p - 2r_p$ . From the above equality,  $L$  can be calculated. Knowing  $L$ , the right radius at which one loop can just form is obtained. (Since volume fraction is known). The rate of shrinkage of a single loop of this radius is calculated from the velocity equation,

$$v = v^* \exp \left[ \frac{-D}{\tau_b - \gamma_{APB} + \frac{L_T}{L}} \right] \quad (46)$$

where  $L_T$  is the line tension.

Case (ii). When two loops can just form

The diameters of the second loops for different particle sizes are calculated from given experimental creep stress. The second loop is assumed to form for a particle size at which  $L$  for the two loop case is equal to  $L$  of the one loop case. Now for this particle size the velocity of the

inner most loop is computed using the equation,

$$v = v^* \exp \left[ \frac{-D}{\tau_b - \gamma_{APB} + L_T + \tau_j \cdot b} \right] \quad (47)$$

where  $\tau_j$  is the stress due to the second loop on the first given by eqn. (27).

The same procedure is adopted for the 3<sup>rd</sup>, 4<sup>th</sup> and 5<sup>th</sup> loops.

The shrinkage rate of the inner most loop is now-determined at different stages of shrinkage and thus the total time to collapse is estimated. It is assumed that this shrinkage time for the inner most loop is also the time taken for one dislocation to travel from one particle to the next. The creep rate is now given by,

$$\text{Creep rate} = \rho b \bar{v} \quad (48)$$

$\rho$  being the mobile dislocation density,  $\bar{v}$  which is velocity of the dislocation in moving from one particle to the other is now,

$$\bar{v} = \frac{\text{distance between precipitates}}{\text{time for shrinkage of the inner loop}} \quad (49)$$

This approach can also be used to estimate the stress dependence (n) of creep rate

$$n = \frac{\tau}{\dot{\epsilon}} \frac{d\dot{\epsilon}}{d\tau} \quad (50)$$

where  $\dot{\epsilon}$  is the creep rate in shear,  $\tau$  the shear stress.

This approach does not consider the effect of straight dislocations.

## CONCLUSIONS

1. The yield model proposed in this work predicts satisfactorily the relationship between yield strength and particle size.
2. The agreement between the experimental and theoretical yield model is satisfactory in the larger particle size range.
3. The results of the yield model have predicted more realistic values as compared to that of Ashby.
4. Increasing volume fraction of precipitates have clearly shown to shift the yield stress-particle size curves to higher values.
5. The lower work hardening rate in underaged alloys is due to the cutting of precipitate particles by dislocations.
6. The higher work hardening rate in overaged alloys may be attributed to the fact that the dislocations have to bow between particles, this being a more difficult process.
7. The results of the stress relaxation tests indicate that the work hardening in these alloys may be wholly attributed to the internal stresses.
8. Strain rate cycling tests have proved to be unreliable for these materials.
9. A study of dislocation dynamics has shown that while in some alloys partial dislocations dissociate, in others they remain undissociated.

- 8
10. The dynamic theory accounts for stabilisation which is exhibited in some alloys.
  11. The model for studying the dislocation dynamics taking curvature of dislocations into account is an improvement over the earlier ones.
  12. A new theory for creep in overaged alloys has been outlined.



# REFERENCES

- Ashby, M.F., 1966, Phil. Mag. 14, 1157.
- Ashby, M.F., 1968, Proc. Second Bolton Landing Conf. on Oxide Dispersion Strengthening, Bolton Landing 1966, Cordon and Breach.
- Bailey, R.W., 1926, J. Inst. Metal. 35, 27.
- Barret, C.S., and Weertman, J., 1959, Trans. AIME, 215, 838.
- Bilsby, C.F., 1966, Thesis, Cambridge University.
- Blackburn, M.J., 1967, Thesis, Cambridge University.
- Cottrell, A.H., and Aytakin, V., 1950, J. Inst. Metal. 77, 389.
- Clark, B.R. and Pickering, F.B., 1967, JISI, 205, 70.
- Copley, S.M. and Kear, B.H., 1967, Trans. AIME 239, 984.
- Copley, S.M. and Kear, B.H., 1968, Acta. Met. 16, 227
- Dulien, D., and Nutting, J., 1964, "High Alloy Steels", ISI Spec. Rep. 86, 140
- Davies, C.K.L., Davies, P.W. and Wilshire, B.W., 1965, Phil. Mag. 12, 827.
- Ebeling, R. and Ashby, M.F., 1966, Phil. Mag., 13, 804
- Fisher, J.C., Hart, E.W. and Pry, R.H., 1953, Acta. Met. 1, 336.
- Finnce, I., and Heller, W.R., 1959, Creep of Engineering Materials, McCraw Hill.
- Friedel, J., 1964, 'Dislocations', Pergamon Press.
- Foreman, A.J.E. and Makin, J.J., 1967, Can. J. Phys. 45, 511.
- Gibbons, T.B., Swedish Institute of Metals Research, Stockholm Report 64.

- Guard, R.W., 1961, *Acta. Met.*, 9, 163.
- Gleiter, H., and Hornbogen, E., 1965, *Phys. Stat. Sol.* 12, 235.
- Gleiter, H., and Hornbogen, E., 1965, *Phys. Stat. Sol.* 12, 251.
- Garfalo, F., 1965, *Fundamentals of creep and creep rupture in Metals*, MacMillan, N.Y.
- Gupta, I. and Li, J.C.N., 1970, *Mat. Sci. Engg.* 6, 20.
- Cuyot, P., 1971, *Phil. Mag.* 24, 987.
- Herring, J., 1950, *J. Appl. Phys.* 437.
- Hirsch, P.B., 1957, *J. Inst. Metals.* 86, 7.
- Hattersley, H. and Hume-Rothery, W., 1965, "The Constitution of Certain Austenitic Stainless Steels", Final Report, Contract No. EMR/1407.
- Hirsch, P.B. and Kelly, A., 1965, *Phil. Mag.* 12, 881.
- Hirsch, P.B. and Humphreys, F.J., 1970, *Proc. Roy. Soc. Lond. A*, 318, 45.
- Hart, E.W., 1972, *Acta. Met.* 20, 275.
- Irvine, K.J., Llewellyn, D.T., and Pickering, F.B., 1961, *JISI*, 199, 153.
- Ishida, Y. and McLean, D., 1967, *JISI*, 205, 88.
- Jeffrees, Z. and Archer, R.S., 1921, *Chem. and Met. Engg.* 24, 1057.
- Jahnke, E. and Emde, F., 1945, "Tables of Functions with Formulas and Curves", Daves, New York, N.Y., p. 73.
- Johnston, W.G. and Gilman, J.J., 1959, *J. Appl. Phys.* 30, 129.
- Johnston, W.G. and Steim, D.F., 1963, *Acta. Met.* 11, 317.
- Kennedy, A.J., 1963, *Processes of creep and fatigue in Metals*, John Wiley, N.Y.

- hear, B.H. and Pearcey, J., 1965, 66-033, Advanced Materials Research and Development Laboratory, Pratt and Whitney Aircraft, North Haven, Conn.
- Labusch, R., 1964, Z. Metallk., 55, 5.
- Li, J.C.M. and Liu, G.C.T., 1968, Proc. of the Int. Conf. on The Strength of Metals and Alloys, Tokyo, p. 26.
- Lagenborg, R., 1958, J. Mat. Sci., 3, 596.
- Merica, P.D., Waltenberg, R.C. and Scott, H., 1921, Trans. AIME, 64, 41.
- Nott, M.F. and Nabarro, F.R.N., 1940, Proc. Phys. Soc. Lond. 52, 86.
- Mihalisin, J.R. and Decker, R.F., 1960, Trans. AIME, 218, 507.
- McLean, D. and Hale, K.F., 1961, ISI Spec. Rep. 19.
- McLean, D., 1962, Met. Rev., 7, 516.
- Michalak, J.T., 1965, Acta. Met. 13, 213.
- McLean, D., 1966, Rep. Prog. Phys. 29, 1.
- Nabarro, F.R.N., 1948, The Phys. Soc. Lond., 75.
- Noble, F.W. and Hull, D., 1964, Acta. Met. 12, 1089.
- Nicholson, R.B., 1971, ISI Publication No. 145.
- Orowan, E., 1940, Proc. Phys. Soc. 52, 8.
- Orowan, E., 1946, J. West Scot. Iron St. Inst. 54, 45.
- Orowan, E., 1948, "Symposium on Internal Stresses in Metals and Alloys (Institute of Metals), 451.
- Orowan, E., 1954, "Dislocations in Metals", AIME, Ed. N. Cohen, p. 131.

- Philips, V.A., 1967, Trans. AIME, 230, 967.
- Papaleo, R. and Whiteman J.A., 1971, "Effect of Second Phase Particles on the Mechanical Properties of Steel" ISI Publication No. 145, p. 22.
- Rodriguez, P., 1968, J. Mat. Sci. 3, 98.
- Rayner, D. and Silcock, J.M., 1970, J. Met. Sci. J., 4, 121.
- Seeger, A., 1956, "Dislocations and Mechanical Properties of Crystals", Wiley, New York.
- Swann, P.R., 1963, "Electron Microscopy and Strength of Crystals", 947, Interscience.
- Silcock, J.M. and Williams, N.T., 1966, JISI, 204, 1100.
- Sherby, O.D. and Burke, P.M., 1967, "Mechanical behaviour of crystalline solids at elevated temperatures", Progress in Materials Science 13, 325.
- Singhal, L.K. and Martin, J.W., 1967, Scripta Met. 1, 181.
- Singhal, L.K. and Martin, J.W., 1968, Acta. Met. 16, 947.
- Singhal, L.K. 1968, Ph.D. Thesis, Oxford University.
- Singhal, L.K., 1970, Phys. Stat. Sol. (a) 3, K 233.
- Thomas, G., 1963, Acta. Met. 16, 227.
- Weertman, J., 1957, J. Appl. Phys. 28, 1185.
- Wilcox, B.A. and Cluer, A.H., 1966, Trans. AIME, 236, 570.
- Wilson, F.G. and Pickering, F.B., 1969, JISI, 207, 490.
- Williams, K.R. and McLauchlin, J. 1970, J. Mat. Sci. 5, 1063.
- Wilcox, B.A., Clauer, A.H. and McCain, W.S., 1967, Trans. AIME 239, 1791.

APPENDIX-1

Calculations for the loop velocity and Frank-Read stress for particle radius of 490 A°.

Radius of first loop = 490 A°

$\tau_{c_1}$  = Critical stress to form first loop

$\tau_{c_2}$  = " " " second loop

$\tau_{c_3}$  = " " " third loop

$\tau_{c_4}$  = " " " fourth loop

Line tension at 490 A° = 19.6 Kg/mm<sup>2</sup>

$2R_s$  = Interparticle spacing

$v_{11}$  = Velocity of the first loop when  $\gamma_{APB} = 280$  ergs/cm<sup>2</sup>

$v_{12}$  = " " " " "  $\gamma_{APB} = 240$  "

$v_{13}$  = " " " " "  $\gamma_{APB} = 200$  "

$v_{14}$  = " " " " "  $\gamma_{APB} = 160$  "

$\tau$  = Applied shear stress

$r_2$  = radius of second loop

$r_3$  = radius of third loop

$r_4$  = radius of fourth loop

When only one loop is present it does not shrink for all

$\gamma_{APB}$  values and  $\tau_{c_1} = 7.03$  Kg/mm<sup>2</sup>,  $2R_s = 3240$  A°.

## Appendix-1 (Contd.)

When second loop forms.

$\tau$ (Kg/mm <sup>2</sup> )	$\tau_{c2}$ (Kg/mm <sup>2</sup> )	$r_2$ (A°)	$v_{11}$ (cm/sec)	$v_{12}$ (cm/sec)	$v_{13}$ (cm/sec)	$v_{14}$ (cm/sec)
6	7.83	579	-	-	-	.187x10 <sup>-8</sup>
7	7.81	575	-	-	-	.232x10 <sup>-5</sup>
8	7.79	573	-	-	-	.665x10 <sup>-4</sup>
9	7.78	570	-	-	S	.168x10 <sup>-2</sup>
10	7.76	567	-	-	S	.206x10 <sup>-1</sup>
11	7.74	565	-	-	S	.101

When third loop forms.

$\tau$ (Kg/mm <sup>2</sup> )	$\tau_{c3}$ (Kg/mm <sup>2</sup> )	$v_1$ (cm/sec)	$v_2$ (cm/sec)	$v_3$ (cm/sec)	$v_4$ (cm/sec)
6	8.82	-	S	.512x10 <sup>-3</sup>	F
7	8.74	-	S	.152x10 <sup>-1</sup>	F
8	8.69	-	S	.121	F
9	8.63	-	.909x10 <sup>-8</sup>	.773	F
10	8.58	-	.423x10 <sup>-4</sup>	F	F
11	8.53	S	.773x10 <sup>-3</sup>	F	F

## Appendix-1 (Contd.)

When fourth loop forms.

$\tau$ (Kg/mm <sup>2</sup> )	$\tau_{c_4}$ (Kg/mm <sup>2</sup> )	$v_1$ (cm/sec)	$v_2$ (cm/sec)	$v_3$ (cm/sec)	$v_3$ (cm/sec)
6	8.84	S	$.982 \times 10^{-4}$	F	F
7	8.66	S	$.101 \times 10^{-1}$	F	F
8	8.52	S	$.987 \times 10^{-1}$	F	F
9	8.39	$.124 \times 10^{-7}$	.772	F	F
10	8.26	$.378 \times 10^{-4}$	F	F	F
11	8.15	$.225 \times 10^{-2}$	F	F	F

APPENDIX-2

## Shrinkage of a loop of radius 250 Å

Loop Radius (Å)	Velocity (cm/sec)	Time to shrink to 50 Å (secs)
250	$.312 \times 10^{-1}$	$6 \times 10^{-5}$
200	$.981 \times 10^2$	$5.1 \times 10^{-9}$
150	$.336 \times 10^4$	$1.49 \times 10^{-10}$
100	$.242 \times 10^5$	$2.07 \times 10^{-11}$

Thus it is seen that at radius below 200 Å the loop shrinks very rapidly and hence the time involved is very small. In calculating the shrinkage rate of the first loop, it is assumed that till the first loop shrinks no new loop forms.



APPENDIX-3

Data on effective, internal and applied stresses  
as a function of strain

Sample Temp. (°C)	Aged at Time (Hrs.)	Strain (percent)	Applied stress (Kg/mm <sup>2</sup> )	Internal stress (Kg/mm <sup>2</sup> )	Effective stress (Kg/mm <sup>2</sup> )
675	20	2.00	53.758	52.4	1.358
		4.10	61.4	59.77	1.63
		5.00	64.45	62.68	1.77
		8.00	71.1	69.2	1.9
		9.5	75.4	73.5	1.9
		10.5	77.9	75.73	2.17
		11.5	80.3	78.13	2.17
		13.2	85.1	82.0	3.1
675	125	2.50	50.6	48.97	1.63
		3.20	58.5	56.7	1.8
		3.90	62.45	60.2	2.25
		5.60	69.1	66.5	2.6
675	550	0.71	40.26	39.0	1.26
		1.40	63.80	62.4	1.4
		2.70	75.8	74.0	1.8
		5.1	85.5	83.0	2.5
		6.9	91.3	88.8	2.5
725	4	1.5	50.85	49.6	1.25
		1.7	51.595	50.1	1.495
		3.9	59.73	58.1	1.63
		6.1	65.32	63.15	2.17
		9.1	71.57	69.15	2.42
725	30	0.3	35.69	34.205	1.485
		1.00	50.5	48.95	1.65
		1.90	57.86	55.8	2.06
		2.6	60.71	58.23	2.48
		3.8	64.93	62.45	2.48
		10.1	81.99	78.55	3.44

## Appendix-3 (Contd.)

725	200	0.45	36.42	35.58	0.84
		2.10	59.08	57.4	1.68
		3.5	64.2	62.1	2.1
		6.3	72.35	69.8	2.55
		8.5	79.8	76.5	3.3
750	1000	2.5	49.19	46.81	2.38
		3.5	56.7	53.9	2.8
		5.0	63.7	60.9	2.8
		8.1	73.29	69.65	3.64
750	200	3.15	51.9	49.9	2.0
		5.8	61.3	58.8	2.5
		9.12	68.3	65.5	2.8
		18.32	79.1	75.59	3.51

APPENDIX-4

Strain rate cycling data on a sample aged at 725°C for 30 hours

Symbols used:

$\dot{\epsilon}_1$  = initial cross head speed

$\dot{\epsilon}_2$  = increased cross head speed

$P_1$  = load at initial strain rate

$P_2$  = load at increased strain rate

$m$  = dislocation velocity stress exponent

$m = \Delta \ln \dot{\epsilon} / \Delta \ln \tau$

$\tau^*$  = effective stress

$\tau_i$  = internal stress

$\tau_A$  = applied stress

Strain (pct)	$\Delta P$ (Kg)	$\log P_2/P_1$	$m$	$\tau^*$	$\tau_A$	$\tau_i$
2.464	2	0.004	99.28	44.4	59.6	15.1
3.74	2	0.0038	104.4	44.4	63.4	19.0
5.97	2	0.0035	113.4	44.4	68.1	23.7
8.3	2	0.0034	116.8	44.4	72.0	27.6
10.07	2	0.0033	120.3	44.4	74.55	30.15
12.92	2	0.0032	124.1	44.4	77.6	33.2

From a plot of  $m$  vs. strain,  $m^*$  is obtained by extrapolating to zero strain.  $m^*$  in this case turns out to be 88.5.

## APPENDIX-5

DISJOINTNESS INTO PARTIALS.

1. Let  $A$  and  $B$  be two sets.

2. Let  $C$  be a set.

3. Let  $D$  be a set.

4. Let  $E$  be a set.

5. Let  $F$  be a set.

6. Let  $G$  be a set.

7. Let  $H$  be a set.

8. Let  $I$  be a set.

9. Let  $J$  be a set.

10. Let  $K$  be a set.

11. Let  $L$  be a set.

12. Let  $M$  be a set.

13. Let  $N$  be a set.

14. Let  $O$  be a set.

15. Let  $P$  be a set.

16. Let  $Q$  be a set.

17. Let  $R$  be a set.

18. Let  $S$  be a set.

19. Let  $T$  be a set.

20. Let  $U$  be a set.

21. Let  $V$  be a set.

22. Let  $W$  be a set.

23. Let  $X$  be a set.

24. Let  $Y$  be a set.

25. Let  $Z$  be a set.

26. Let  $A$  and  $B$  be two sets.

27. Let  $C$  be a set.

28. Let  $D$  be a set.

29. Let  $E$  be a set.

30. Let  $F$  be a set.

31. Let  $G$  be a set.

32. Let  $H$  be a set.

33. Let  $I$  be a set.

34. Let  $J$  be a set.

35. Let  $K$  be a set.

36. Let  $L$  be a set.

37. Let  $M$  be a set.

38. Let  $N$  be a set.

39. Let  $O$  be a set.

40. Let  $P$  be a set.

41. Let  $Q$  be a set.

42. Let  $R$  be a set.

43. Let  $S$  be a set.

44. Let  $T$  be a set.

45. Let  $U$  be a set.

46. Let  $V$  be a set.

47. Let  $W$  be a set.

48. Let  $X$  be a set.

49. Let  $Y$  be a set.

50. Let  $Z$  be a set.

$$A_1 = \begin{pmatrix} 1 & 0 \\ 0 & 1 \end{pmatrix} \text{ and } A_2 = \begin{pmatrix} 1 & 0 \\ 0 & 0 \end{pmatrix}$$
[illegible][illegible]

1. *Chlorophyll a* (Chl *a*)

... ..

Figure 1. The effect of the concentration of the *Agrobacterium* suspension on the transformation efficiency of *Agrobacterium* strains.

2 4 6

100

[illegible]

Case	Age	Gender	Site
1	65	Male	Stomach
2	65	Male	Stomach
3	65	Male	Stomach
4	65	Male	Stomach
5	65	Male	Stomach
6	65	Male	Stomach
7	65	Male	Stomach
8	65	Male	Stomach
9	65	Male	Stomach
10	65	Male	Stomach
11	65	Male	Stomach
12	65	Male	Stomach
13	65	Male	Stomach
14	65	Male	Stomach
15	65	Male	Stomach
16	65	Male	Stomach
17	65	Male	Stomach
18	65	Male	Stomach
19	65	Male	Stomach
20	65	Male	Stomach
21	65	Male	Stomach
22	65	Male	Stomach
23	65	Male	Stomach
24	65	Male	Stomach
25	65	Male	Stomach
26	65	Male	Stomach
27	65	Male	Stomach
28	65	Male	Stomach
29	65	Male	Stomach
30	65	Male	Stomach
31	65	Male	Stomach
32	65	Male	Stomach
33	65	Male	Stomach
34	65	Male	Stomach
35	65	Male	Stomach
36	65	Male	Stomach
37	65	Male	Stomach
38	65	Male	Stomach
39	65	Male	Stomach
40	65	Male	Stomach
41	65	Male	Stomach
42	65	Male	Stomach
43	65	Male	Stomach
44	65	Male	Stomach
45	65	Male	Stomach
46	65	Male	Stomach
47	65	Male	Stomach
48	65	Male	Stomach
49	65	Male	Stomach
50	65	Male	Stomach
51	65	Male	Stomach
52	65	Male	Stomach
53	65	Male	Stomach
54	65	Male	Stomach
55	65	Male	Stomach
56	65	Male	Stomach
57	65	Male	Stomach
58	65	Male	Stomach
59	65	Male	Stomach
60	65	Male	Stomach
61	65	Male	Stomach
62	65	Male	Stomach
63	65	Male	Stomach
64	65	Male	Stomach
65	65	Male	Stomach
66	65	Male	Stomach
67	65	Male	Stomach
68	65	Male	Stomach
69	65	Male	Stomach
70	65	Male	Stomach
71	65	Male	Stomach
72	65	Male	Stomach
73	65	Male	Stomach
74	65	Male	Stomach
75	65	Male	Stomach
76	65	Male	Stomach
77	65	Male	Stomach
78	65	Male	Stomach
79	65	Male	Stomach
80	65	Male	Stomach
81	65	Male	Stomach
82	65	Male	Stomach
83	65	Male	Stomach
84	65	Male	Stomach
85	65	Male	Stomach
86	65	Male	Stomach
87	65	Male	Stomach
88	65	Male	Stomach
89	65	Male	Stomach
90	65	Male	Stomach
91	65	Male	Stomach
92	65	Male	Stomach
93	65	Male	Stomach
94	65	Male	Stomach
95	65	Male	Stomach
96	65	Male	Stomach
97	65	Male	Stomach
98	65	Male	Stomach
99	65	Male	Stomach
100	65	Male	Stomach

1. *Chlorophyll a* (Chl *a*)

1990

1. The first group of people who are not in the labor force are those who are not in the labor force for any reason. This group includes people who are not in the labor force because they are not in the labor force for any reason. This group includes people who are not in the labor force because they are not in the labor force for any reason.

1. *Chlorophyll a* and *Chlorophyll b* were determined by the method of Arar and Collins (1971) using a Shimadzu 1601 UV-Visible Spectrophotometer.

1. The first step in the process is to identify the problem or issue that needs to be addressed. This involves gathering information and understanding the context of the problem.

1. The first part of the document is a list of names and dates, which appears to be a roster or a list of participants. The names are written in a cursive script, and the dates are written in a more formal, printed style. The list is organized into two columns, with names on the left and dates on the right.

**Figure 6.** The effect of the number of trials on the mean accuracy of the responses ( $n = 10$ ) for each condition. Error bars represent standard error of the mean.

1. *Journal of the American Medical Association*, 1997; 277: 1033-1038.

— 10 —

1. *Chlorophyll a* (Chl *a*)

[illegible]

1000

10	11	12	13	14	15	16	17	18	19	20	21	22	23	24	25	26	27	28	29	30	31	32	33	34	35	36	37	38	39	40	41	42	43	44	45	46	47	48	49	50	51	52	53	54	55	56	57	58	59	60	61	62	63	64	65	66	67	68	69	70	71	72	73	74	75	76	77	78	79	80	81	82	83	84	85	86	87	88	89	90	91	92	93	94	95	96	97	98	99	100
----	----	----	----	----	----	----	----	----	----	----	----	----	----	----	----	----	----	----	----	----	----	----	----	----	----	----	----	----	----	----	----	----	----	----	----	----	----	----	----	----	----	----	----	----	----	----	----	----	----	----	----	----	----	----	----	----	----	----	----	----	----	----	----	----	----	----	----	----	----	----	----	----	----	----	----	----	----	----	----	----	----	----	----	----	----	----	----	----	----	-----

100

10

1987 2 1987

1990

Circumstance	Percentage (%)
Self-defense	85
To protect others	75
To prevent a crime	65
To punish a criminal	45

1000

Figure 1. The effect of the concentration of the *Agaricus bisporus* spores on the growth of *Agaricus bisporus* on the substrate. The concentration of the spores was 10<sup>4</sup> spores/g (a), 10<sup>5</sup> spores/g (b), 10<sup>6</sup> spores/g (c), 10<sup>7</sup> spores/g (d), 10<sup>8</sup> spores/g (e), 10<sup>9</sup> spores/g (f), 10<sup>10</sup> spores/g (g), 10<sup>11</sup> spores/g (h), 10<sup>12</sup> spores/g (i), 10<sup>13</sup> spores/g (j), 10<sup>14</sup> spores/g (k), 10<sup>15</sup> spores/g (l). The substrate was 100 g of the substrate. The concentration of the spores was 10<sup>4</sup> spores/g (a), 10<sup>5</sup> spores/g (b), 10<sup>6</sup> spores/g (c), 10<sup>7</sup> spores/g (d), 10<sup>8</sup> spores/g (e), 10<sup>9</sup> spores/g (f), 10<sup>10</sup> spores/g (g), 10<sup>11</sup> spores/g (h), 10<sup>12</sup> spores/g (i), 10<sup>13</sup> spores/g (j), 10<sup>14</sup> spores/g (k), 10<sup>15</sup> spores/g (l).

100 200 300 400 500 600 700 800 900 1000

100

1000

## APPENDIX-6

Separation of partials as obtained by the modified dynamic theory (present work).

Constants used:

$$\begin{aligned}\gamma_m &= 15 \text{ ergs/cm}^2 & \gamma_p &= -200 \text{ ergs/cm}^2 \\ r_s &= 30 \text{ \AA} & 2R_s &= 140 \text{ \AA} \\ \gamma_{APB} &= 280 \text{ ergs/cm}^2 & \Delta x &= 150 \text{ \AA} \\ v^* &= 2.52 \times 10^5 \text{ cm/sec} & D_m &= 475 \text{ ergs/cm}^2 \\ D_p &= 867 \text{ ergs/cm}^2 & \gamma_{bp} &= 59 \\ \cos \phi/2 &= .2472 \\ \phi &= 151.4 \\ \phi &= 14.3\end{aligned}$$

Initial contact length = 25  $\text{\AA}$

$d_p$  = distance between trailing and leading partial  
in contact with precipitate

$d_m$  = distance between trailing and free segment of  
the leading partial

$d_p$ ( $\text{\AA}$ )	$d_m$ ( $\text{\AA}$ )
86.8	88.8
19.34	45.3
19.34	65.3
29.34	50.3
10.5	40.1

It is seen that dissociation occurs under these conditions